

PDF issue: 2025-10-27

Automated Segmentation of Bones and Muscles in the Hip and Thigh from X-ray Computed Tomography Scans

Yokota, Futoshi

```
(Degree)
博士 (工学)
(Date of Degree)
2015-03-06
(Date of Publication)
2016-03-01
(Resource Type)
doctoral thesis
(Report Number)
乙第3280号
(URL)
https://hdl.handle.net/20.500.14094/D2003280
```

※ 当コンテンツは神戸大学の学術成果です。無断複製・不正使用等を禁じます。著作権法で認められている範囲内で、適切にご利用ください。



神戸大学博士論文

Automated Segmentation of Bones and Muscles in the Hip and Thigh from X-ray Computed Tomography Scans (X線断層画像を用いた股関節および大腿部の筋骨格自動領域分割)

平成 27 年 1 月

横田 太

Automated Segmentation of Bones and Muscles in the Hip and

Thigh from X-ray Computed Tomography Scans

Futoshi Yokota

Abstract

The computer-aided diagnosis and surgery (CAD/CAS) has become increasingly common. Understanding of the behavior of the musculoskeletal system may lead to further advancement of CAD/CAS. In order to understand the behavior of the musculoskeletal system, patient-specific biomechanical simulations of the bones and muscles have been proved to be useful. In order to perform a patient-specific simulation, 3-dimensional model of the target anatomy (e.g., bones and muscle) constructed by segmentation in medical images obtained from each individual is essential. The ultimate goal of our research is to automate segmentation of anatomical structures such as the bones and muscles in medical images to obtain the complete understanding of those anatomies. In this thesis, I specifically focus on segmentation of the bones and muscles with emphasis on the hip and thigh from x-ray computed tomography (CT).

Localization of the pelvic anatomical coordinate system is prerequisite of patient specific preoperative planning and joint motion simulation for hip surgery. Our aim is to automate localization of the pelvic anatomical coordinate system from 3D CT data. In this thesis, a statistical atlas based method is proposed that consists of three steps. The first step is spartial normalization using probabilistic atlas. The second step is feature points recognition using a statistical landmark model. The final step is coordinate system refinement using average CT atlas. I applied the proposed method to 39 datasets. Compared to the manual localization by one experienced surgeon, average position error was 2.37 ± 1.30 mm and orientation error was 1.07 ± 0.50 degrees, which demonstrates usefulness of the proposed method.

I present a fully automatic method to segment hip joint from CT image with a specific focus on diseased hips, where the fused joint washes out the image features and challenges accurate segmentation. Our approach makes strong use of two types of statistical shape models (SSMs): the hierarchical SSM and conditional SSM. Both SSMs were constructed in the training phase and sequentially applied in the segmentation phase to systematically hone-in on the region of interest, i.e., joint surface, by eliminating other confounders that might otherwise cause erroneous segmentation. Surface subdivisions for the hierarchical and conditional SSM were determined without manual supervision using the canonical correlation analysis that calculates significance of correlation between two points. The proposed framework was evaluated through the segmentation of one hundred female patients (200 hemi-hips) who had underwent total hip arthroplasty. The patients were classified into five disease categories and the hip joints were manually traced by experienced surgeons, which comprised a wellorganized ground-truth dataset for training and testing of the proposed method. Two-fold cross validation studies revealed the average symmetric surface distance of 1.30 ± 0.81 mm for the diseased acetabulum, 1.30 ± 0.72 mm for the diseased femoral head with the proposed method while 1.78 ± 1.61 mm, 1.72 ± 1.00 mm with the conventional method where individual SSM was employed. The proposed method was most effective in severely worn joints, which suggested that the systematic approach effectively decreased the generality and increased specificity in segmentation phase. The accurate segmentation in diseased hips provides quantitative information for quality assurance in treatment planning.

Patient-specific biomechanical simulations using image-based musculoskeletal modeling have been proved to be useful. However, time-consuming nature in image segmentation of muscles is an obstacle to their clinical application. In this thesis, we propose a fully-automated method for segmentation of muscles from hip CT data whose FOV covers the entire pelvis and femur. The feature of the proposed method is hierarchical strategy using hierarchical nature inherent in the musculoskeletal anatomy. The evaluation was performed

using the ground truth on three representative 2D axial slices of 10 CT datasets in a leaveone-out manner. The average absolute distance error of segmented 17 muscles was 3.1 mm for the proposed and 4.2 mm for the simplified methods, respectively.

In this thesis, I accomplished an automated segmentation of the bones and muscles in the hip and thigh from x-ray computed tomography. Proposed method consist of three parts: 1) recognition of the anatomical landmarks, 2) segmentation of the bones (pelvis and femur), 3) segmentation of the muscles (seventeen individual muscles). Our future work also includes: 1) application to different anatomies (e.g. knee, shoulder, etc.) and different modalities (e.g. MRI), 2) application to the musculoskeletal simulation including a model of muscle fibers and considering the porosity difference between cortical bone and trabecular bone.

Contents

1	Intr	oductio	n	1	
2	Auto	Automated Localization of Pelvic Anatomical Coordinate System from 3D CT			
	Data	a of the	Hip Using Statistical Atlas	6	
	2.1	Introdu	uction	8	
	2.2	Metho	d	10	
		2.2.1	Definition of pelvic anatomical coordinate system	10	
		2.2.2	Overview of pelvic anatomical coordinate system automatically lo-		
			calization	10	
		2.2.3	Removal of unnecessary space area and normalized using a proba-		
			bilistic atlas	12	
		2.2.4	Recognition of anatomical landmarks using a statistical model fea-		
			ture points	17	
		2.2.5	Refinement of pelvic anatomical coordinate system using the pubic		
			symphysis average image	20	
	2.3	Results	s	22	
		2.3.1	Experimental condition	22	
		2.3.2	Experimental results	23	
	2.4	Discus	sion	26	

	2.5	Conclu	ision	29
3	Auto	omated CT Segmentation of Diseased Hip Using Hierarchical and Condi-		
	tion	al Statis	etical Shape Models	30
	3.1	Introdu	action	32
	3.2	Materi	als	35
	3.3	Methods		38
		3.3.1	Overview of the proposed framework	38
		3.3.2	Localization of pelvic anatomical landmarks using statistical learning	39
		3.3.3	Learning phase	39
	3.4	Segme	ntation phase	46
	3.5	Results	S	49
		3.5.1	Experimental conditions	49
		3.5.2	Experimental results	51
	3.6	Discus	sion	62
	3.7	Conclu	isions	65
4	Auto	mated	CT Segmentation of Muscles Using Hierarchical Multi-Atlas method	67
	4.1	Introdu	action	69
	4.2	Methods		69
		4.2.1	Overview	69
		4.2.2	Hierarchical multi-atlas label fusion	70
		4.2.3	Application to hip and thigh musculoskeletal segmentation	71
	4.3	Results	S	72
	4.4	Discus	sion and conclusions	73
5	Con	clusions	S	76

List of Figures

1.1	Musculoskeletal models proposed in a prior work (Left: [1], Right: [2]	4
1.2	VOXEL-MAN. This figure was taken from [3]	5
2.1	Definition of anatomical pelvic coordinate system. Left: Frontal view (Anterior-	
	Posterior direction). Right: Side view (Lateral-Medial direction)	11
2.2	Overview of proposed method	12
2.3	Field of view (FOV) and coordinate system of 3D-CT image. Left: Coronal	
	view of CT image. Right: Visualization of FOV and coordinate system	14
2.4	Construction of probabilistic atlas. (a) Lower limit of the pelvis. (b) Upper	
	limit of the femur. (c) Cylinder region including spine. Left: Three examples	
	from training dataset. Right: Constructed probabilistic atlases	16
2.5	Construction of statistical landmark model. (a) Three examples from training	
	dataset. (b) Variation models of constructed statistical landmark model	18
2.6	Construction of mid pubic average image. (a) Three examples from training	
	dataset (axial image). (b) Constructed average image. Left: Axial image.	
	Middle: Coronal image. Right: Sagittal image	21
2.7	Effects of tangent plane constraint (w_1) and average arrangement constraint	
	(w_2) . Upper: Positional error. Lower: Orientation error	25
2.8	Estimation accuracy for different voxel size and matrix size of average image.	26

2.9	Two examples of typical results. The red coordinate system is automatically	
	estimated results. The blue coordinate system is gold standard. (a) Typical	
	successful case. (b) Illustrative case showing effects of probabilistic atlas	27
3.1	CT images of the representative cases. (a) and (b) Coronal and axial slices.	
	The window and level for all images are 800 and 400 HU. (c), (d) and (e) 3D	
	renderings of the hip, pelvis and femur.	37
3.2	Overview of proposed method	38
3.3	Hierarchical hip SSM. Anatomy-based separation is performed in second	
	level. CCA-based separation is performed in third or lower level	41
3.4	The extent of sub-region representing the acetabulum and femoral head de-	
	termined by CCA. (a) p-value map on the basis of CCA of the femur sur-	
	face influenced by the pelvis and the pelvis surface influenced by the femur.	
	Smaller values indicate stronger correlation with the adjacent bone. (b) The	
	acetabulum and femoral head region obtained by the corresponding p-value	
	threshold	43
3.5	The extent of sub-region representing the acetabulum and femoral head de-	
	termined by CCA. (a) p-value map on the basis of CCA of the femur sur-	
	face influenced by the pelvis and the pelvis surface influenced by the femur.	
	Smaller values indicate stronger correlation with the adjacent bone. (b) The	
	acetabulum and femoral head region obtained by the corresponding p-value	
	threshold	44

3.6	The first mode of the standard and conditional FH-SSM and A-SSM. The	
	upper two rows show SSMs of the acetabulum for two different patients (re-	
	ferred to as case 1 and case2), while the lower two rows are the femoral	
	head. In each case, a coronal slice overlaid with contour lines of $+2\sigma$, mean,	
	and -2 σ surfaces is shown at the left column and the other three columns	
	show 3D visualization of each surface. The standard SSMs are the same for	
	both cases, since there is no constraint from segmentation of the other bone.	
	Conditional SSMs for both cases are change by target contour	45
3.7	Dependency of the threshold value on ASD in the hip bone that was used for	
	tuning of the threshold value in the first level of hierarchical SSM	52
3.8	Dependency of the threshold value on ASD in the acetabulum and femoral	
	head that was used for tuning of the threshold value in the second level of	
	hierarchical SSM	53
3.9	ASD as a function of the two parameters: p-value in determination of the	
	condition surface using CCA and $\boldsymbol{\gamma}$ in ridge regression. The dotted points	
	are the sample points at which the ASD values were actually computed and	
	the colormap shows linear interpolation between the sample points. The	
	dashed red lines indicate the minimum value	54
3.10	Boxplots showing segmentation accuracy of diseased and unaffected hips. *	
	and **: significant improvement; *: $0.01 , **: p < 0.01$	56
3.11	Boxplots showing segmentation accuracy for each disease category in the	
	acetabulum and femora head. * and **: significant improvement; *: $0.01 <$	
	$p < 0.05, **: p < 0.01. \dots$	57

3.12	Segmentation results of the representative case of each disease category.	
	Case 1, 2, 3, and 4 correspond to osteoarthritis, crowe 1, crowe 2 and col-	
	lapsed hip, respectively. (a) coronal slices at the plane of the approximate	
	femoral center. The green and red contours correspond to the segmented re-	
	gions of the pelvis and femur, respectively. Arrows in (a) indicate the part	
	where segmentation accuracy improved with the hierarchical and conditional	
	SSM. (b) and (c) 3D rendering of the segmented surface with colormap in-	
	dicating the surface distance error.	58
3.13	Segmentation results of the representative case of each disease category.	
	Case 1, 2, 3, and 4 correspond to osteoarthritis, crowe 1, crowe 2 and col-	
	lapsed hip, respectively. (a) coronal slices at the plane of the approximate	
	femoral center. The green and red contours correspond to the segmented re-	
	gions of the pelvis and femur, respectively. Arrows in (a) indicate the part	
	where segmentation accuracy improved with the hierarchical and conditional	
	SSM. (b) and (c) 3D rendering of the segmented surface with colormap in-	
	dicating the surface distance error	59
3.14	Segmentation results of the representative case of each disease category.	
	Case 1, 2, 3, and 4 correspond to osteoarthritis, crowe 1, crowe 2 and col-	
	lapsed hip, respectively. (a) coronal slices at the plane of the approximate	
	femoral center. The green and red contours correspond to the segmented re-	
	gions of the pelvis and femur, respectively. Arrows in (a) indicate the part	
	where segmentation accuracy improved with the hierarchical and conditional	
	SSM. (b) and (c) 3D rendering of the segmented surface with colormap in-	
	dicating the surface distance error.	60

4.1	Schematic diagram of hip and thigh musculoskeletal segmentation processes	
	using hierarchical multi-atlas label fusion	7 4
4.2	Typical cases of muscle segmentation. (a) Body (skin), pelvis, and femur. (b)	
	Muscle tissues. (c) 17 individual muscles. Left: Proposed method. Right:	
	Simplified method. (d) Axial slices of segmentation results of individual	
	muscles. Left: Proposed method. Middle: Manual traces. Right: Simplified	
	method	75
5.1	An example sectioned slice in Visible Korean Human (VKH).	78

List of Tables

2.1	Average error and standard deviation of estimation error	24
2.2	Average positional and orientation errors for different weight values w_1 (tan-	
	gent plane constraint) and w_2 (average arrangement constraint)	24
3.1	Number of cases in each disease category	36
3.2	Specification of the CT scanning	36
3.3	Evaluation results for segmentation accuracy of diseased and unaffected hips.	
	Mean and standard deviation of ASDs [mm] are shown in each method. The	
	best results are shown in a bold font	55
3.4	Evaluation results for the acetabulum segmentation accuracy of disease cate-	
	gory. Mean and standard deviation of ASD [mm] in each category are shown	
	for each method. The best results are shown in bold. * and **: significant	
	improvement; *: $0.01 , **: p < 0.01$	61
3.5	Evaluation results for segmentation accuracy of whole pelvis and femur.	
	Mean and standard deviation of ASDs over two hundreds dataset are shown	
	in each method. The best results are shown in bold. * and **: significant	
	improvement; *: $0.01 , **: p < 0.01$	62

Chapter 1

Introduction

Evidence-based medicine (EBM) based on the computer-aided diagnosis and therapy has become increasingly common. Understanding of the behavior of the musculoskeletal system may lead to further advancement of EBM.

In order to understand the behavior of the musculoskeletal system, patient-specific biomechanical simulations of the bones and muscles have been proved to be useful. Some literature reported effectiveness of the simulation of the bones in surgical planning for the cases such as the bone fracture [4], hip surgery [5, 6], bone loss [7]. Other literatures evaluated simulation of the muscle fiberss in [1, 8, 2] (Fig. 1.1).

In order to perform a patient-specific simulation, 3-dimensional model of the target anatomy (e.g., bones and muscle) constructed by segmentation in medical images obtained from each individual is essential. Voxel-Man is one of the state-of-the-art human model including musculoskeletal structures which was constructed by Hohne et al. [9]. In Voxel-Man project, the model was constructed from a series of images of one patient that was manually segmented (Fig. 1.2). Generally, image segmentation of bones and muscles is time-consuming and prone to inter-operator variability, which creates severe challenges for a patient-specific simulation in clinical routine.

The ultimate goal of our research is to automate segmentation of anatomical structures such as the bones and muscles in medical images to obtain the complete understanding of those anatomies. In this thesis, I specifically focus on segmentation of the bones and muscles with emphasis on the hip and thigh from x-ray computed tomography (CT). The research group which the author was involved has been engaging in the development of an automated planning system for total hip arthroplasty (THA) surgery (i.e., an orthopaedic surgery of the hip joint), thus we selected the hip and thigh as the target anatomy in this study. X-ray CT is almost completely free from geometrical distortion and non-homogeneity of intensity values compared to magnetic resonance images (MRI). Furthermore, x-ray CT is one of the most widespread modality in orthopaedic surgery in Japan because it provides high contrast at

bone boundaries.

The novelty of this thesis over the prior works is that this work achieved a fully automated segmentation of the musculoskeletal system in the hip and thigh from CT image for the first time.

This thesis consists of five chapters. The brief overview of each chapter is as follows: Introduction (this chapter) is described in Chapter 1, recognition of the anatomical landmarks is described in Chapter 2, segmentation of the hip bones (pelvis and femur) is described in Chapter 3, segmentation of the muscles (seventeen individual muscles) is described in Chapter 4, and Chapter 5 concludes the thesis.

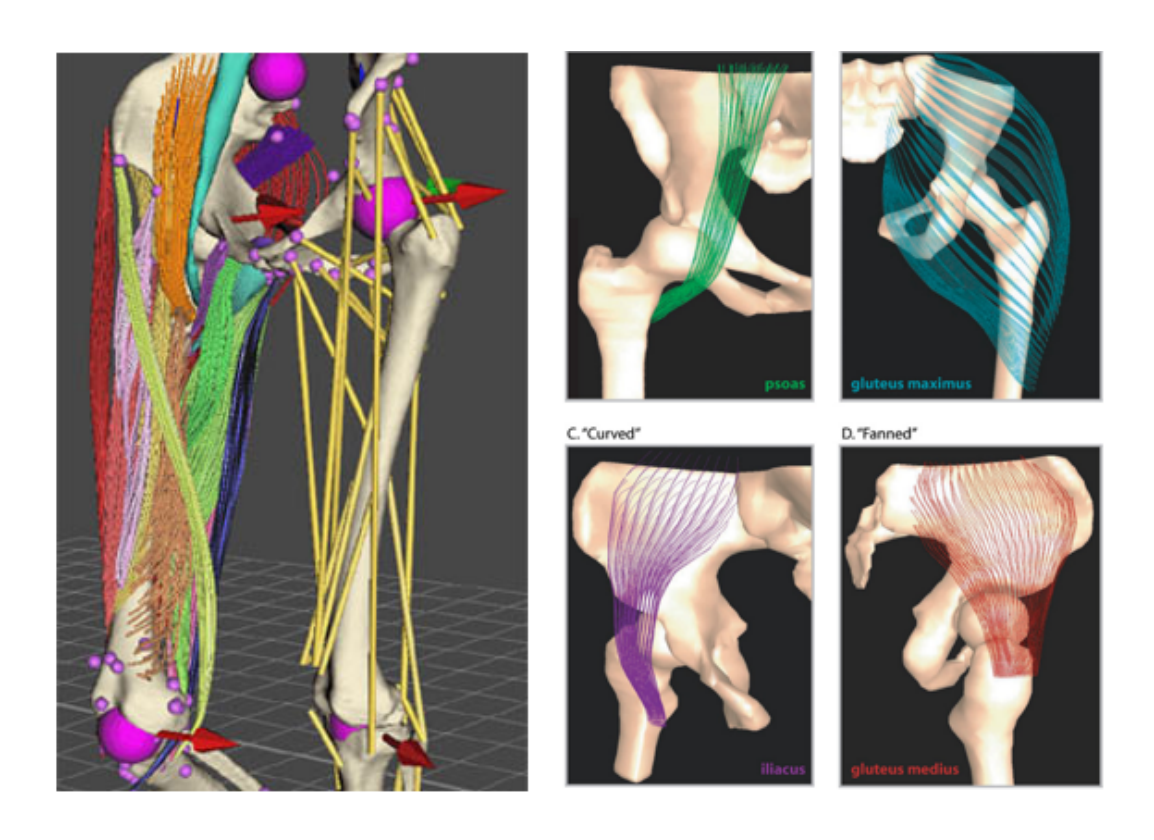


Figure 1.1: Musculoskeletal models proposed in a prior work (Left: [1], Right: [2].



Figure 1.2: VOXEL-MAN. This figure was taken from [3].

Chapter 2

Automated Localization of Pelvic

Anatomical Coordinate System from 3D

CT Data of the Hip Using Statistical Atlas

Abstract

Localization of the pelvic anatomical coordinate system is prerequisite of patient specific preoperative planning and joint motion simulation for hip surgery. Our aim is to automate localization of the pelvic anatomical coordinate system from 3D CT data. In this thesis, a statistical atlas based method is proposed that consists of three steps. The first step is spartial normalization using probabilistic atlas. The second step is feature points recognition using a statistical landmark model. The final step is coordinate system refinement using average CT atlas. We applied the proposed method to 39 datasets. Compared to the manual localization by one experienced surgeon, average position error was 2.37 ± 1.30 mm and orientation error was 1.07 ± 0.50 degrees, which demonstrates usefulness of the proposed method.

2.1 Introduction

In surgical navigation system for a hip, a surgical planning system and dynamics simulations [6], in order to define the position of the prosthesis and the orientation of the femur relative to the pelvis [10][11], setting the pelvic coordinate system is necessary. The setting of the pelvic coordinate system is effective to initialize the area extraction using statistical shape model [12]. I am building the automated preoperative planning system for a total hip replacement. By currently, manually input the pelvis coordinate system, I can automatically segmentation of the femur and pelvis [12] and planning of surgical planning [6] inclusing articulation simulation. Automates the pelvis coordinate system setting, with the aim to build a system of fully automatic, to address the automation of the pelvis coordinate system set in this thesis.

Automatic method of setting the pelvic coordinate system some have been proposed. Method for automatically estimating (Anterior Pelvic Plane. Subsequent abbreviated as APP) pelvic plane has been proposed before as a reference plane of the pelvic coordinate system [13]. In this approach, APP seeking plane tangent to the bone shape. However, there is a possibility that APP crosses the femur and the spine depending on the posture of the hip joint, adversely affects the estimation of the tangent plane. Method is set by deforming to the patient data atlas pelvic shape as a different method, set the anatomical landmarks in advance is proposed. In the method of aligning a patient data reference atlas using a non-rigid transformation [14] can not be performed properly non-rigid registration of the cases the deformation is large, it becomes necessary to manually correct the results. The method of applying the three-dimensional ultrasound image statistical shape model (SSM [15]), the target image is an ultrasound image, and is taken selectively only image of anatomical landmarks near required for configuring APP [16]. Therefore, when it is applied to CT images this technique, it is necessary to manually set the range of anatomical landmarks near, can not

be automated immediately. In the above-mentioned techniques [13][14][16], pelvic shape is assumed to be symmetric, and sets the median plane with the midpoint of the left and right pubic tubercle. However, the disease is a hip surgery subject, since it is the shape is not symmetrical, it may be desirable to determine the median plane from the midpoint of the left and right pubic tubercle is not appropriate. In addition, these studies are few cases of application number of cases, it can not be said enough validation is being performed.

In this thesis, we propose an automatic method of setting the pelvis coordinate system using statistical atlas. Statistics atlas used are the following three.

- Probabilistic atlas [17]
- Statistical landmark model
- Average image

First, the deletion of a region that adversely affect APP set and the femoral region and the spine by using a probabilistic atlas. Next, the recognition of pelvic anatomical landmarks using a statistical model feature points. It is expected that for statistical feature point model is a brief model of four-point anatomical landmarks used for configuring APP, is hardly affected by the shape of the anatomical landmarks other than in the vicinity. In addition, since the variation of the posture is included, it is robust against imaging posture. Finally, to carry out refinement of the pelvic anatomical coordinate system using the average image of the pubic symphysis near the lateral center of the pubic tubercle. The use of image information, it is possible to determine the median plane without being influenced by the asymmetric shape based diseases.

2.2 Method

2.2.1 Definition of pelvic anatomical coordinate system

Definition of the pelvis coordinate system, their definition or pelvis anatomical coordinate system, such as a number is an anatomical definition as a reference the Anterior Pelvic Plane (APP) [18], valid International Society of Biomechanics of (ISB) defined in the mechanical analysis field [19] or valid functional coordinate system [20]. In this thesis, for use as the initial value of the segmentation pelvis, the femur region to target pelvic anatomical coordinate system.

Figure 1 shows the definition of pelvic anatomical coordinate system. Here, the lateral direction, Y axis is the cranio-caudal direction longitudinal and Z-axis X-axis. Is set as the XZ plane before pelvic plane is the plane containing the pubic tubercle forward-projecting point and anterior superior iliac spine on the left and right. Anterior Pelvic Plane (APP) include the anterior superior iliac spine and most anterior point of pubic tubercle set as XZ-plane X-axis axis is defined an connecting the anterior superior iliac spine on the left and right. To the coordinate system origin to the point obtained through projection of the APP and the pubic symphysis. Z axis is defined which is perpendicular to the X axis on APP. Y-axis is determined from the respective axes and obtained above.

2.2.2 Overview of pelvic anatomical coordinate system automatically localization

Figure 2.2 shows an overview of the pelvis anatomical coordinate system automatically localization. This method is composed of a two-step fully automatic set-up phase of the pelvic anatomical coordinate system using a statistical atlas built with construction stage of the statistical atlas is a learning process in advance. Statistics atlas built in the learning stage are

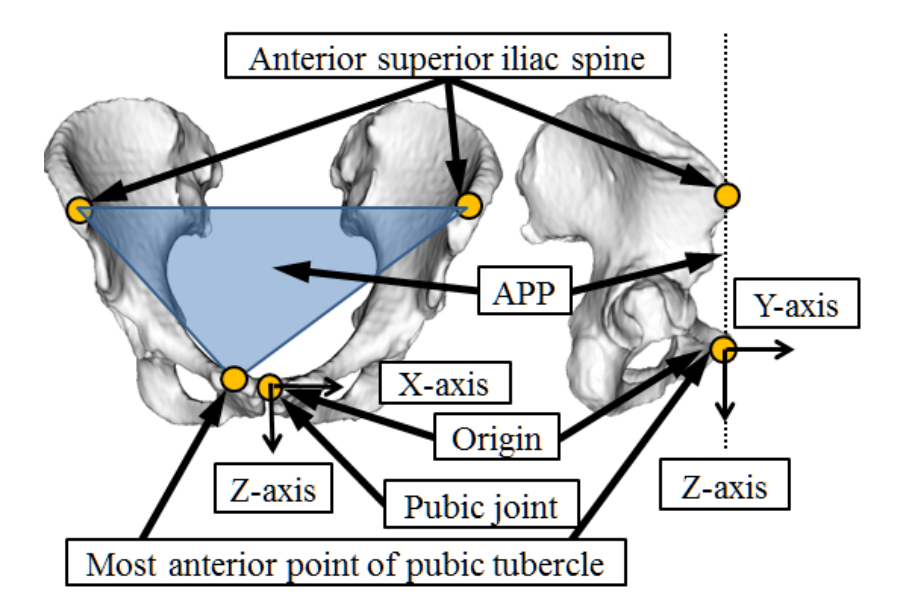


Figure 2.1: Definition of anatomical pelvic coordinate system. Left: Frontal view (Anterior-Posterior direction). Right: Side view (Lateral-Medial direction).

three as follows.

- Probabilistic atlas
- Statistical landmark model
- Average image

To perform fully automatic settings pelvic anatomical coordinate system and apply the following processing with respect to the bone tissue area that is extracted by rough thresholding, using a statistical atlas built.

- 1. Removal of unnecessary space area and normalized using a probabilistic atlas
- 2. Recognition of anatomical landmarks using a statistical model feature points
- Refinement of pelvic anatomical coordinate system using the pubic symphysis average image

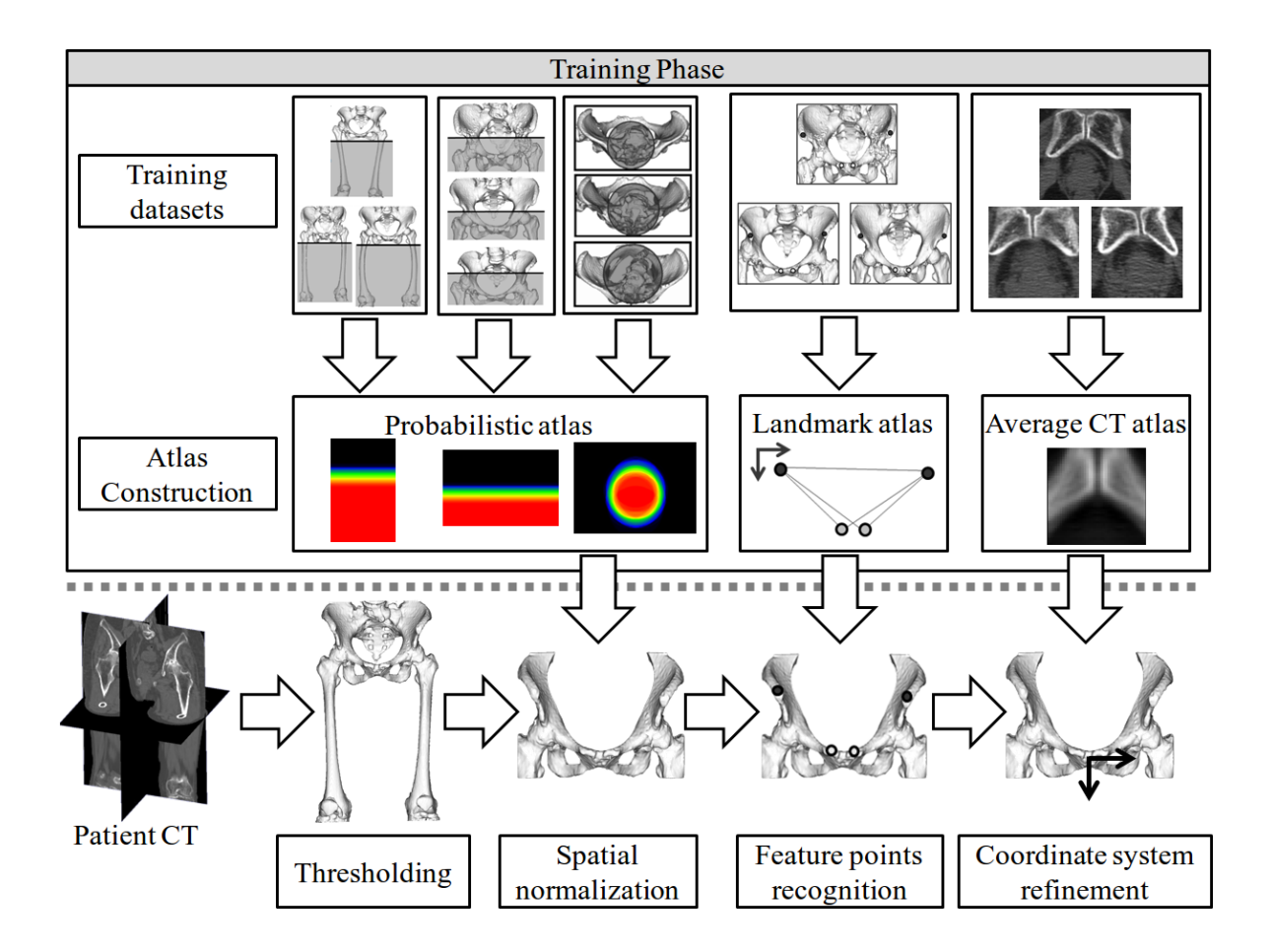


Figure 2.2: Overview of proposed method.

I described in subsequent sections for automatic processing method using a statistical atlas built and how to build a statistical atlas.

2.2.3 Removal of unnecessary space area and normalized using a probabilistic atlas

m

Spatial normalization is required in order to utilize the statistical feature point model described in Section 2.4. In this method, the use of the pelvic area circumscribed rectangular

space to normalization. Using a probabilistic atlas to determine automatically the pelvic region circumscribed rectangular, but in the construction of the probabilistic atlas, normalization of the input data is required. In this section, you will CT imaging range and have been taken to lower end of the femur from the pelvis top in a supine position, first, this FOV probability atlas to find the front and rear left and right ends of the pelvis as the normalized space (Field of view) (pelvis lower end I want to build a probabilistic atlas) of the upper femur high-level and high-level area below the lower region. That is, is used as the reference coordinate system the CT coordinate system (Fig. 2.3). Then, I want to build a (probabilistic atlas of the spine area) Atlas probability of obtaining the pelvis top as normalized space circumscribed rectangular solid of the pelvis around the left and right ends. Probabilistic atlas of the spinal region of only being normalized space circumscribed rectangular pelvic fro end, because the remains of the CT coordinate system, the variation of the position of the spine is too large. I describe how to remove unwanted sites and space normalization using a probabilistic atlas built and how to build a probabilistic atlas below.

Probabilistic atlas construction: Probabilistic atlas is constructed from n training dataset. Let x is the three-dimensional coordinates of the normalized space. In the image of the cases i was mapped to normalized space, let a binary image to be 0 pixel value if the target area is not present as 1 pixel value if the target area is present, probabilistic atlas P(x) is defined as following equation.

$$P(x) = \frac{1}{n} \sum_{i=1}^{n} B_i(\mathbf{x})$$
(2.1)

A probabilistic atlas is constructed for the following regions:

- Pelvis lower end of the high-level lower region : $P_{pelvis}(x_{ct})$
- Femur top high lower region : $P_{femur}(x_{ct})$
- Spine region : $P_{spine}(x_{pelvis_xy})$

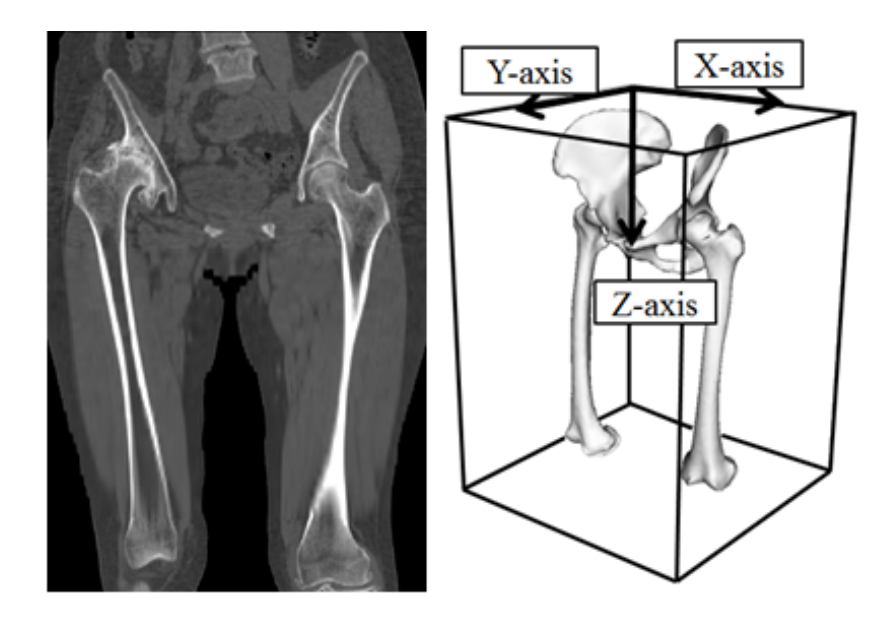


Figure 2.3: Field of view (FOV) and coordinate system of 3D-CT image. Left: Coronal view of CT image. Right: Visualization of FOV and coordinate system.

Here, x_{ct} is coordinate in the normalized space and x_{pelvis_xy} is coordinate coordinate of the normalized space by rectangular bounding of the pelvis front, back, left and right end there. The lower pelvic area below the high-level probability atlas $P_{femur}(x_{ct})$ is used in order to determine the pelvis front and rear end and lower end of the pelvis. The femoral upper high-level lower region probabilistic atlas $P_{femur}(x_{ct})$ is used to determine the left and right ends pelvis. The spinal region probabilistic atlas $P_{spine}(x_{pelvis_xy})$ is used to determine the upper pelvis.

Figure 2.4 show a probabilistic atlas and the example of learning data. Each $P_{pelvis}(x_{ct})$ and $P_{femur}(x_{ct})$ are automatically constructed from the pelvis and femur region traced manually. $P_{spine}(x_{pelvis_xy})$ is constructed automatically from the cylindrical region which is manually set according to the CT coordinate system Z axis to include the spinal region. In the CT image the FOV, it builds from the binary image to be 1, 0 and high present a pixel value of the high order pelvis does not exist. Similarly, $P_{femur}(x_{ct})$ builds from the binary image

to be high order one, does not exist the pixel values of the high order femur there is 0. The pelvis around the left and right ends circumscribed rectangular space, $P_{spine}(x_{pelvis_xy})$ builds from the binary image to position cylinder along the CT coordinate system Z axis, including the spine there is a zero position where the pixel value of 1, does not exist.

Probabilistic atlas application: The estimation of the pelvic circumscribed rectangular, is performed by removing the unnecessary area by using a probabilistic atlas constructed. First, using $P_{pelvis}(x_{ct})$, areas that do not exist pelvic learning all data, that is, remove the region to be the $P_{pelvis}(x_{ct})=1$ in . Fig. 2.4(a). Deleting the femoral region by examining the maximum number of connected components bone area for each slice from the bottom of the area obtained. Many connected components is two-component, since many connected components is 3 or more components, a region not including the pelvis as a 2 connected components in the regions including the femur and pelvis in the slice only femur present remove. Here, the front and rear ends of the pelvis and the lower bounding rectangular solid is obtained . Next, using $P_{pelvis}(x_{ct}) = 1$, area in which there is the femur in one case in the training data of all , that is, remove the region to be the $P_{femur}(x_{ct})$ in . Fig. 2.4(b). Here , it is possible to remove the femoral region exists outside the left and right ends of the pelvis , the left and right ends of the pelvis circumscribed rectangular is obtained. Finally, in the space that has been normalized by the circumscribed rectangular solid of the pelvis around the left and right ends, area where there is area of the spine even one case in learning all data using $P_{spine}(x_{pelvis_xy})$, namely Fig. 2.4(c) to delete a region to be $P_{spine}(x_{pelvis_xy}) > 0$. By removing the spinal region is bone that is present above the pelvis imaging within the CT image of interest, the upper end of the pelvic circumscribed cuboid unit, pelvic circumscribed rectangular is set. Recognition of pelvic anatomical landmarks using a statistical model feature points I discuss automated method of recognizing anatomical landmarks using a statistical feature point model built with building a statistical model feature points in space which is normalized by the pelvic region circumscribed rectangular.

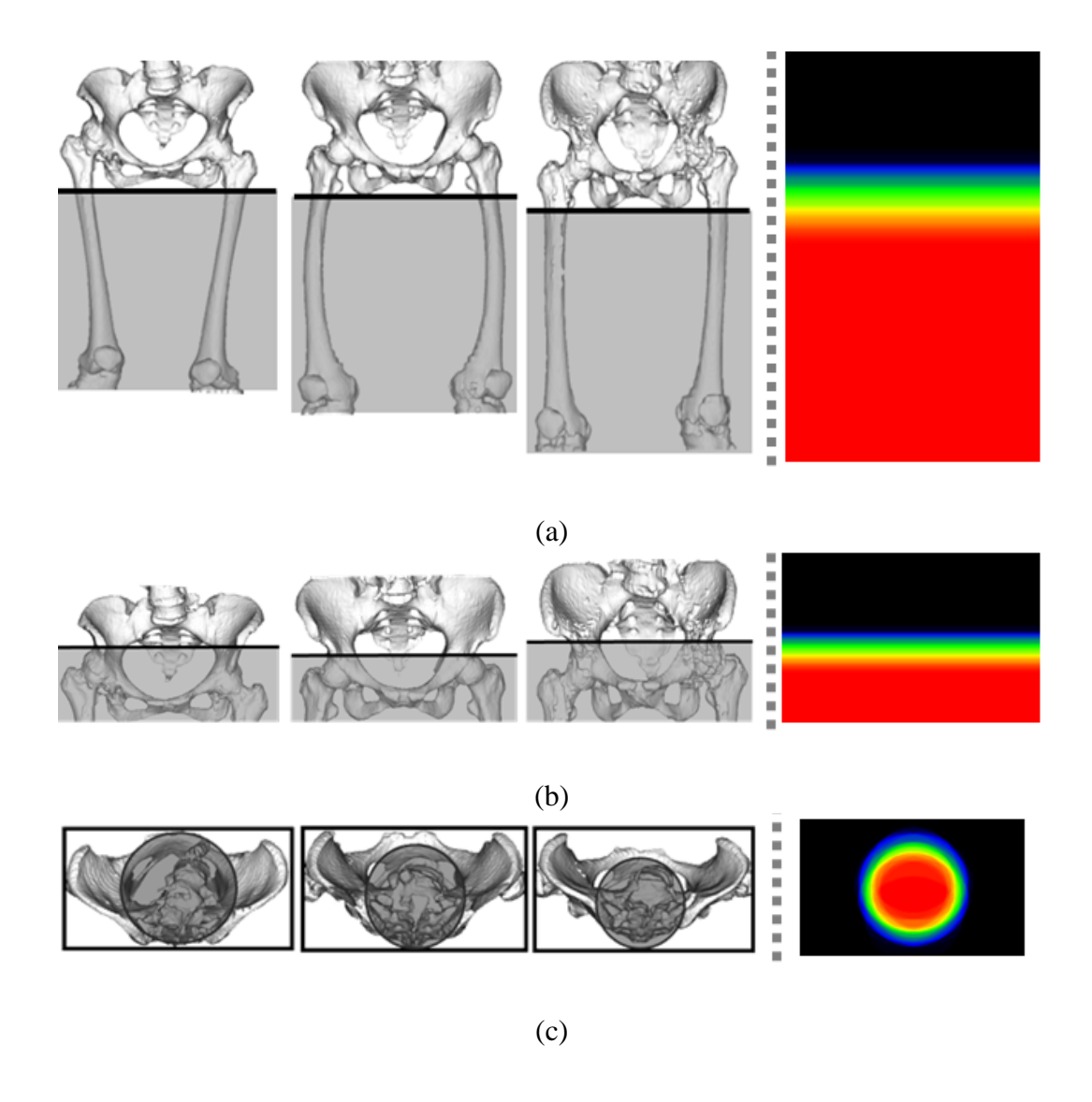


Figure 2.4: Construction of probabilistic atlas. (a) Lower limit of the pelvis. (b) Upper limit of the femur. (c) Cylinder region including spine. Left: Three examples from training dataset. Right: Constructed probabilistic atlases.

2.2.4 Recognition of anatomical landmarks using a statistical model feature points

I describe automated method of recognizing anatomical landmarks using a statistical feature point model built with building a statistical model feature points in space which is normalized by the pelvic region circumscribed rectangular.

Statistics landmark model building: Feature points used to construct the statistical model feature point is four points of the right and left pubic tubercle and anterior superior iliac spine on the right and left to be used for setting of APP. Normalizing the scale pelvic region circumscribing rectangular of each training data, to match the pelvic circumscribing rectangular data used as a reference. Let $q_i(i=1,\cdots,n)$ is 12-dimensional vector of the three-dimensional coordinates of four points. By applying the principal component analysis for the feature point vector group q_i of n cases, to calculate the eigenvector matrix Φ and the 12 eigenvalues $\lambda_l(l=1,\cdots,12)$. Statistical model feature points to be built is expressed by the following equation.

$$\mathbf{q}(\mathbf{b}) = \bar{\mathbf{q}} + \mathbf{\Phi}\mathbf{b} \tag{2.2}$$

Here, $\bar{\bf q}$ is the average arrangement of the feature points, ${\bf b}$ is coefficients for eigenvectors (hereinafter referred to as a shape parameter). It is possible within the variation of the learning data to generate an arbitrary arrangement of the feature points by varying the shape parameter ${\bf b}$. For each of the first principal component, the second principal component, Fig. 2.5 shows how the change in the statistical model of the feature point when it was changed in the range of $\pm 2\sigma$ coefficients (σ is standard deviation).

Statistics landmark model application: I describe the estimation method of anatomical landmarks using statistical feature point mode. In normalization of the pelvic space circumscribed rectangular solid, to obtain bone tissue area which you removed the spine area using $P_{spine}(x_{pelvis_xy})$ from the bone tissue area that is roughly extracted by thresholding. Performs

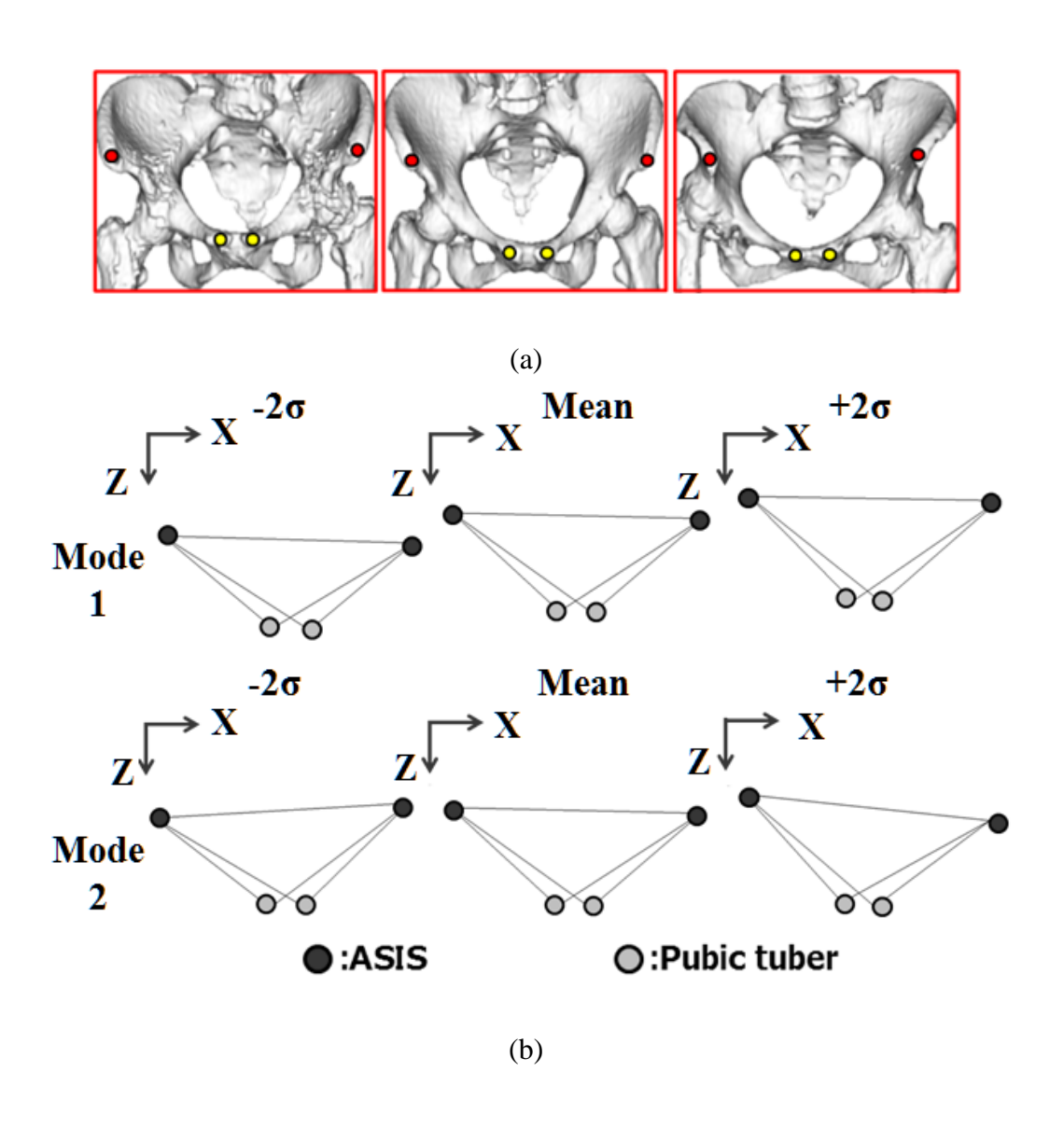


Figure 2.5: Construction of statistical landmark model. (a) Three examples from training dataset. (b) Variation models of constructed statistical landmark model.

a polyhedral approximation to a region obtained using the Marching Cubes method, and further, to reconstruct the surface shape S is thinned vertices vertices so that the number of the point m. $s_k(k=1,\cdots,m)$ is the vertices of S. Let the plane P APP set by three points at the midpoint of the left and right pubic symphysis and the anterior superior iliac spine on the left and right of the statistical model feature points. If S is given, it is optimized using the Levenberg-Marquardt method, the shape parameter \mathbf{b} of the statistical model feature points so as to minimize the cost function below.

$$C(\mathbf{b}; \mathbf{q}(\mathbf{b}), \mathbf{S}) = \mathbf{C_1}(\mathbf{q}(\mathbf{b}), \mathbf{S}) + \mathbf{w_1}\mathbf{C_2}(\mathbf{S}, \mathbf{P}) + \mathbf{w_2}\mathbf{C_3}(\mathbf{b})$$
(2.3)

where,

$$C_1(\mathbf{q}(\mathbf{b}), \mathbf{S}) = \frac{1}{4} \sum_{j=1}^{4} \mathbf{d}(\mathbf{q}_j(\mathbf{b}), \mathbf{S})^2$$
(2.4)

$$C_2(S, P) = \frac{1}{m} \sum_{k=1}^{m} d_+(\mathbf{s_k}, \mathbf{P})^2$$
 (2.5)

$$d_{+} = \begin{cases} d(\mathbf{s_k}, \mathbf{P}) & (\mathbf{s_k} \text{ is anterior position of } \mathbf{P}) \\ 0 & (\mathbf{s_k} \text{ is posterior position of } \mathbf{P}) \end{cases}$$
(2.6)

$$C_3(\mathbf{b}) = \frac{1}{12} \sum_{l=1}^{12} \frac{\mathbf{b}_l^2}{\lambda_l}$$
 (2.7)

Here, $C_1(\mathbf{q}(\mathbf{b}), \mathbf{S})$ is the sum of squares of the distance to the nearest point of the bone surface shape \mathbf{S} , that is, the cost for the APP is in contact with the bone shape from the four points of the statistical model feature points. $d(\mathbf{x}, \mathbf{S})$ is a function for obtaining the distance to the nearest point of the surface shape S of the point \mathbf{x} . $C_2(S, P)$ is the sum of squares of the distance to the nearest point of the plane P, ie from the top of the bone surface shape S which is present in front of the plane P is the APP which is set from four points of the statistical feature point model (hereinafter, referred to as the tangent plane constraints APP)

is a constraint term to ensure that the APP is not filled in bone shape , w_1 is its weight . $d_+(\mathbf{s_k},\mathbf{P})$ is a function for obtaining the distance to the nearest point on the plane P from the point y on the front of the plane P. $C_3(\mathbf{b})$ is the sum of the squares of the Mahalanobis distance from the average arrangement , ie (hereinafter , referred to as average placement constraint) is a constraint term to ensure that the statistics feature point model does not deviate significantly from the average placement , w_2 its weight . Number of vertices of the statistical model feature points is four points , since the number of principal components is not as large as 12 at the most , is not performed dimension reduction by main component analysis in the present study , I use all 12 main component . Pelvis coordinate system is set by using the anatomical landmarks that have been estimated .

2.2.5 Refinement of pelvic anatomical coordinate system using the pubic symphysis average image

Performs the position correction of the anatomical feature points estimated by the statistical model feature points, thereby refinement symmetric surface position of the pelvic anatomical coordinate system. I considered for pubic symphysis is near the center of the left and right pubic tubercle is the cartilage, the left and right boundaries of the pelvis is clear, image information and can be effectively utilized. Therefore, to determine the boundaries of the right and left pelvis using the average image of the vicinity of the pubic symphysis.

The construction of the pubic symphysis average image: average image to be used is assumed to be the average of the image around the pubic symphysis of all learning data. Fig. 2.6 showes an average image built. I described in Chapter 3 for the final adjustment of the matrix size and voxel size.

Performing the average image: Let the initial position, the midpoint of the left and right pubic tubercle obtained by fitting statistical models feature points. Is performed (hereinafter,

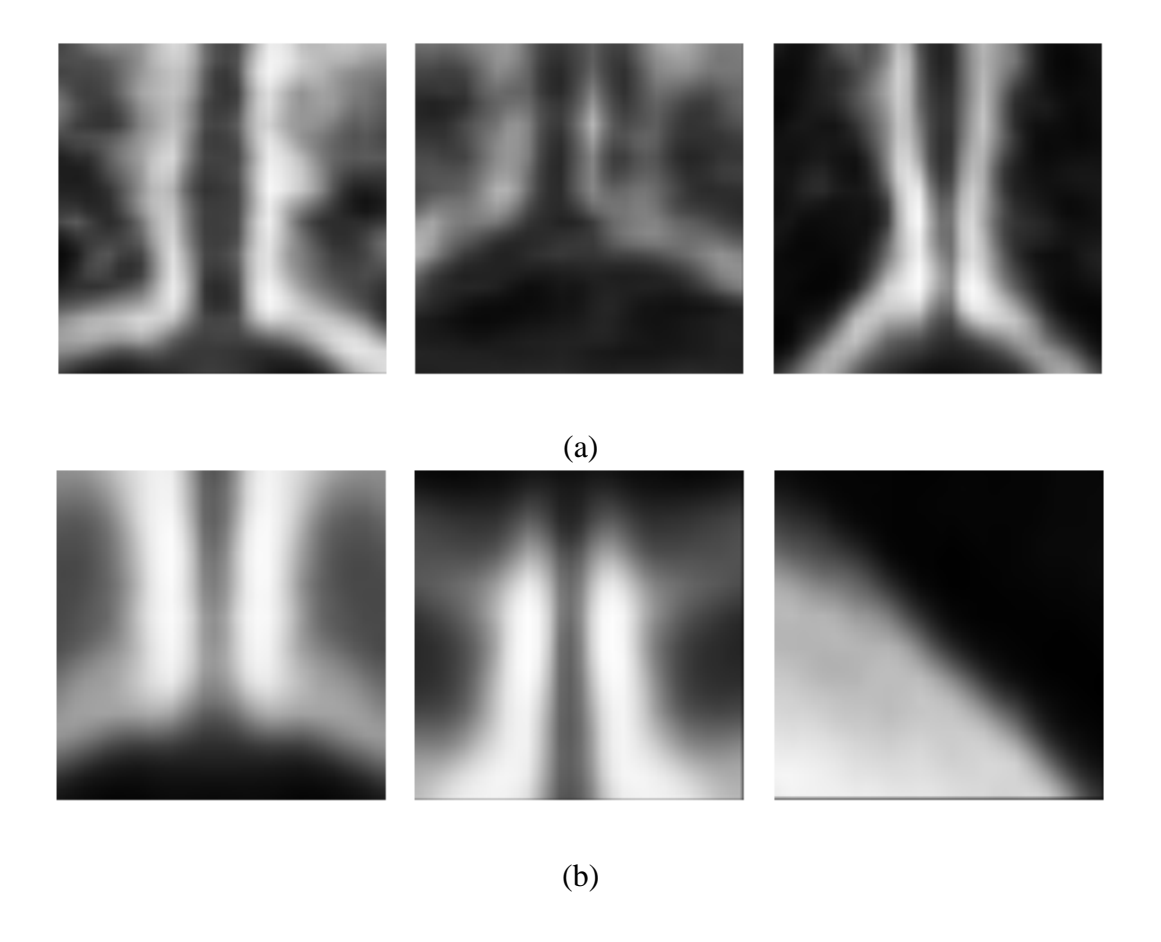


Figure 2.6: Construction of mid pubic average image. (a) Three examples from training dataset (axial image). (b) Constructed average image. Left: Axial image. Middle: Coronal image. Right: Sagittal image.

referred to as the pubic symphysis average image matching) the average image comparison of the pubic symphysis by normalized cross-correlation to the CT image of the initial position around, and the midpoint of the pubic tubercle points with the highest correlation. The result of the statistical fit feature point model, for error, there may not be bone surface shape on the feature point position fit. Therefore, to perform position correction of the feature points and the bone surface shape on and near the anatomical landmarks found in Section 2.4, so that the Y-coordinate minimum pelvic anatomical coordinate system set in Section 2.4.

2.3 Results

To determine the position angle error with pelvic anatomical coordinate system skilled specialist is set, we verified the accuracy of the proposed method.

2.3.1 Experimental condition

As learning data of the statistical atlas construction, I was using the 39 cases of osteoarthritis of the hip that is the subject of a total hip replacement. FOV of the CT image was 360×360 mm, the matrix size iwas 512×512 , pelvic region was 6 mm 2 mm, femoral region slice thickness. Correction pelvic anatomical coordinate system set by the anatomical landmarks skilled specialist enters the surgical plan for the patient. The position error the distance between the origin position of the correct coordinate system and the position of the origin of the coordinate system obtained by the automatic setting, the angle error of the rotation angle difference for each axis, to perform accurate evaluation of Leave-one-out cross-validation were. 150 HU the threshold of bone tissue region extraction. Pubic symphysis average image matching, was probed with 0.5 mm spacing within the cube of one side 40 mm around the pubic symphysis.

2.3.2 Experimental results

Table 2.1 show the (After refinement) estimate the final error that made the refinement by the pubic symphysis and the average image (Before refinement) estimation error of the anatomical coordinate system, which is estimated by statistical feature point model . The estimation error of the pelvic anatomical coordinate system the final position error was 2.37 ± 1.30 mm, the angular error was 1.07 ± 0.50 degrees. The estimation by statistical feature point model, the error in the X-axis direction was 2.54 mm, and 0.60 mm and improvement was observed by the refinement based on the average image. Angular error final was 1.0 degrees in each axis.

Figure 2.7 shows the behavior of the position angle error when changing the value of w_1 the weight w_2 relative to the average placement constraints and the tangent plane constraint. Coordinate system setting accuracy is improved by the co-introduced (Equation 2.4), the average placement constraints tangent plane constraint (Equation 2.5). I used this value for the recognition (Table 2.2), the anatomical landmarks according to the statistical model feature point position angle error is minimized when $w_1 = 0.2$ and $w_2 = 0.02$.

Figure 2.8 shows the results of varying the matrix size and the voxel size of the symphysis pubis average image used for refinement of the feature point position. Position error is minimized when voxel size was $1.0~mm^3$, matrix size was $20 \times 20 \times 20$, I was using these values n the refinement.

Figure 2.9 shows an example estimation of pelvic anatomical coordinate system. Blue color is automatically set coordinate system specialist setting the coordinate system, the red, the green region is a region that is removed by the probabilistic atlas. Cases of Fig. 2.9(a) is a case of the estimation error average. Cases of Fig.2.9(b) is a case in which the spine area exists in front of the APP. It is confirmed that it is possible to set the APP without being affected by the spine across the pelvic tangent plane from this figure.

Table 2.1: Average error and standard deviation of estimation error.

		Before refinement	After refinement
		3.87 ± 2.02	2.37 ± 1.30
	X	2.54 ± 2.02	0.60 ± 0.49
Positional error [mm]	у	0.94 ± 0.62	1.07 ± 0.62
	Z	2.01 ± 1.72	1.83 ± 1.37
		1.21 ± 0.63	1.07 ± 0.50
	X	0.55 ± 0.49	0.50 ± 0.46
Orientation error [degree]	у	0.95 ± 0.60	0.78 ± 0.52
	Z	0.22 ± 0.16	0.19 ± 0.17

Table 2.2: Average positional and orientation errors for different weight values w_1 (tangent plane constraint) and w_2 (average arrangement constraint).

	$w_1 = 0$	$w_1 = 0.2$
$w_2 = 0$	9.73 [mm]	4.40 [mm]
	4.84 [degree]	1.21 [degree]
$w_2 = 0.02$	9.25 [mm]	3.87 [mm]
	4.88 [degree]	1.21 [degree]

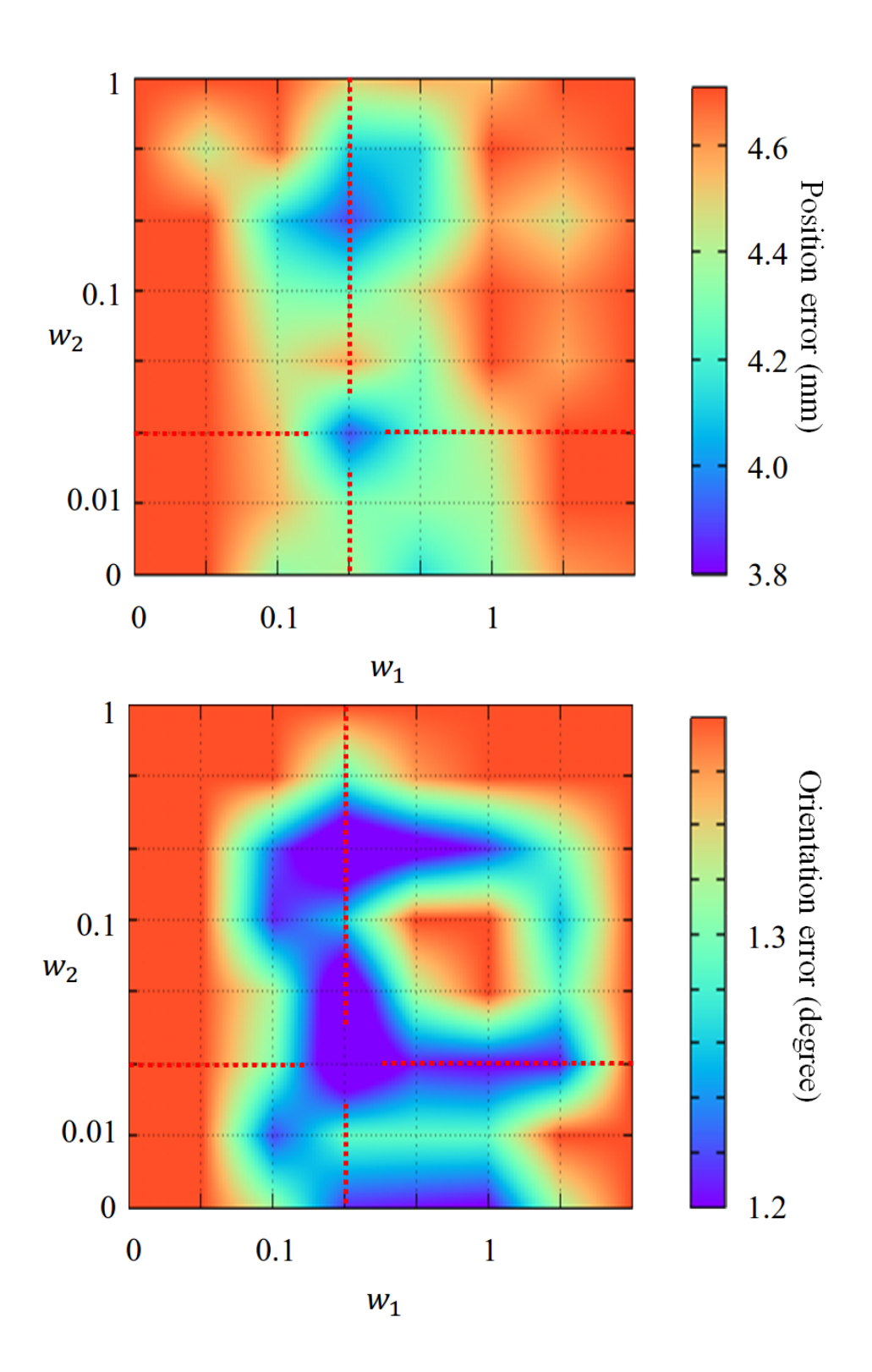


Figure 2.7: Effects of tangent plane constraint (w_1) and average arrangement constraint (w_2) .

Upper: Positional error. Lower: Orientation error.

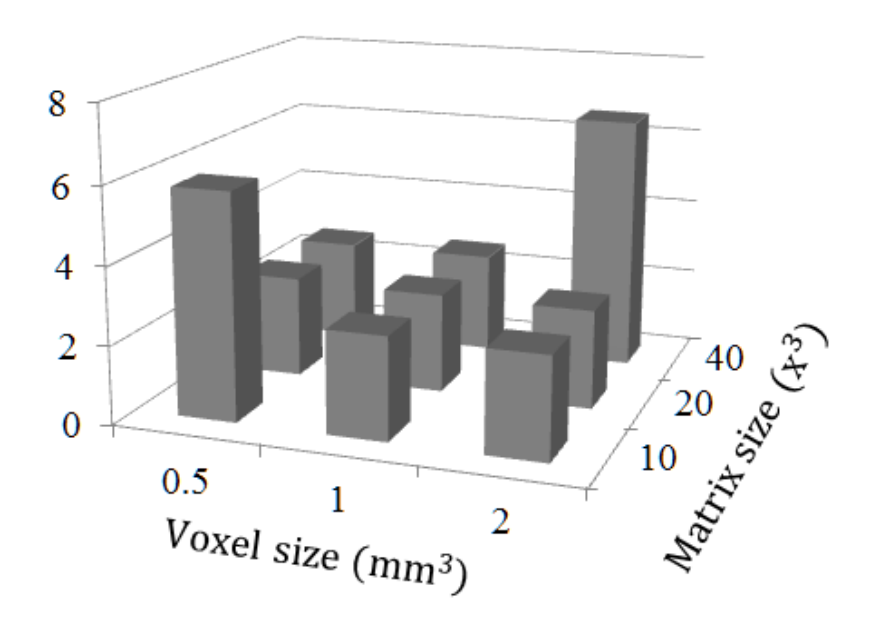


Figure 2.8: Estimation accuracy for different voxel size and matrix size of average image.

2.4 Discussion

I describe the accuracy of pelvic anatomical coordinate system , which is estimated by the proposed method . Consider the fact that the position error of the X-axis direction finally has an error one voxel (0.70 mm) is within 0.60 mm, and to have done with sufficient accuracy to estimate the median plane . I think from that position error in the X-axis direction of the pubic symphysis average image verification before was 2.54 mm, refined by the pubic symphysis average image is alive and functioning . Angular final error is 1.07 degree , and was less than 1 degree in each axis . Since the distance to the rotational center of the hip joint from the coordinate system origin is approximately 100 mm about 1 degree angular error of the Y axis of the coordinate system is about 1.74mm at the center of rotation of the hip joint . The difference between the length of the foot of the left and right are the allowable range is 5.0mm or less in hip surgery , consider 1.74 mm be an error allowed for that . Also , consider

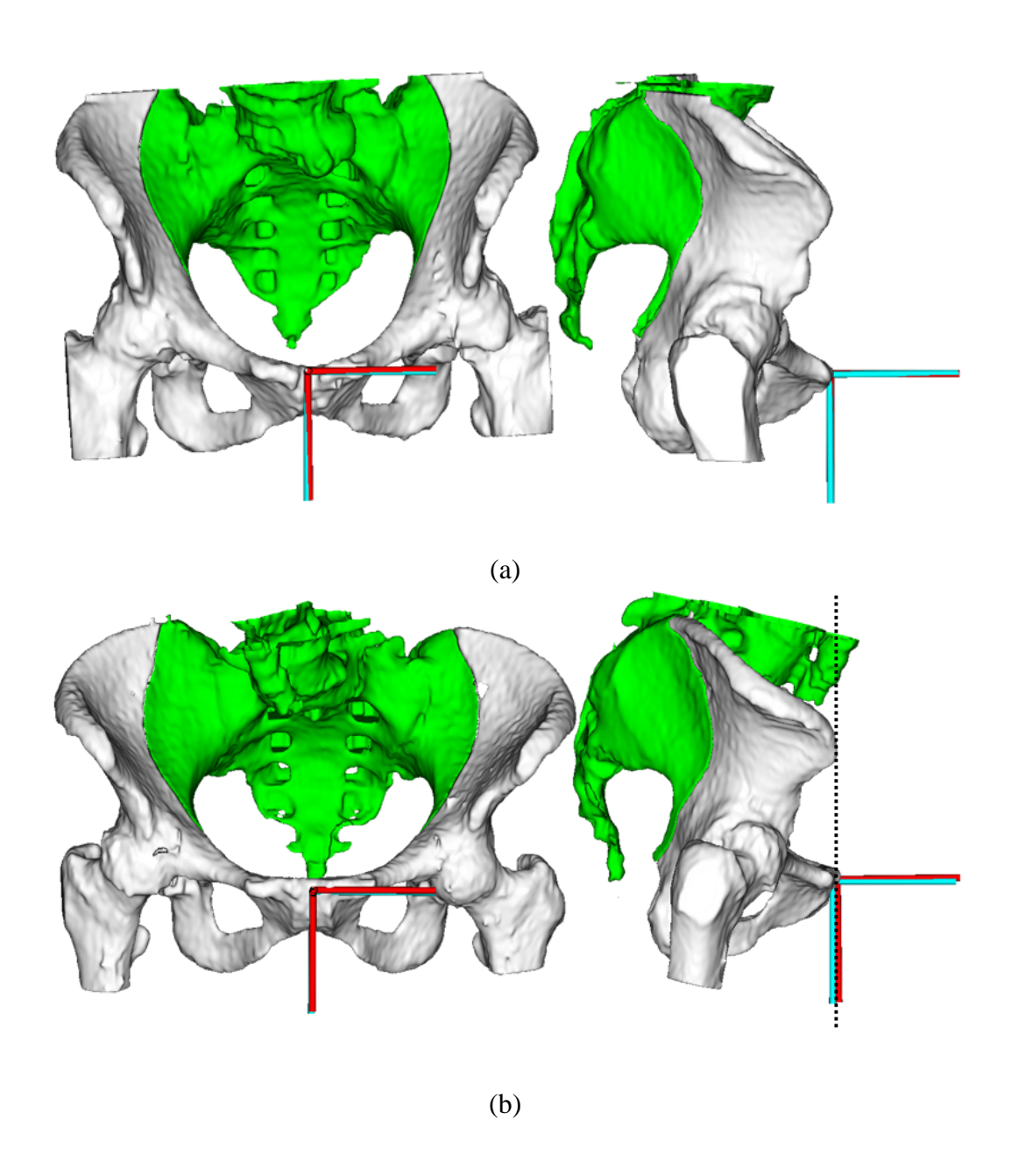


Figure 2.9: Two examples of typical results. The red coordinate system is automatically estimated results. The blue coordinate system is gold standard. (a) Typical successful case. (b) Illustrative case showing effects of probabilistic atlas.

the angular error of each axis is 1 degree or less even coordinate estimation result using the statistical feature point model refinement before, to be effective only in the statistical feature point model, if only the estimation of APP. Position error in the Z-axis direction ultimately is 1.83 mm, the error is large compared to the other axes. This is presumably because in addition to the curvature of the pubic tubercle portion of the bone surface shape is small features topographical low, information for determining the position on the image as the X-axis direction is small. In the prior study, conduct the input of an anatomical feature point specialist of four people determine the APP, verify the variation of the input [13]. Results of the validation are reported error in the Z-axis direction is large at the input of the pubic tubercle. Therefore, since there is ambiguity in the definition of the Z-axis direction of the pubic tubercle, are considered to be within the allowable error in the Z-direction.

I describe the effect of the stabilization term. Consider, as shown in Table 2.2, with the use of the tangent plane constraint, since the reduced 5.33 mm location error of 3.63 degree angular error is found, the tangent plane constraint is alive and functioning. It is considered by using the average placement constraints Similarly, the average placement constraints alive and functioning of the was observed (equivalent angle error) reduction of 0.48 mm location error. As shown in Fig 2.8, since even when there is a change from a value to minimize the square error, estimation error did not change greatly, image size and the voxel spacing in the average image used in the pubic symphysis average image matching, pubic I said that the point of attachment and that can be estimated in a stable manner.

I describe the effect of the probability atlas. In the cases shown in Fig. 2.9(b), it is considered that if for spinal region is present forward of the APP, to determine the plane tangent to the bone shape, a large error is caused, but in this method, using a probabilistic atlas APP is properly estimated because it excludes the green area. I think probability atlas is alive and functioning from this thing.

2.5 Conclusion

In this thesis, we have proposed a automatic method of setting the pelvis anatomical coordinate system from three-dimensional CT image using statistical atlas. It was confirmed that the deletion of an unnecessary region can effectively configuring APP by using a probabilistic atlas. Further, it was confirmed that the recognition of anatomical landmarks is performed in robust to shape and position by using a statistical model feature points. Challenges of the future, is to verify and integration into fully automatic artificial hip surgery planning system, its impact. As mentioned in introduction, a method to plan automatically the optimal placement of the artificial hip joint and automatic method of extracting the pelvis femur region from three-dimensional CT image by entering the pelvis anatomical coordinate system it has been proposed, with the aim of building a system that can fully automatic processing by combining with the proposed method [12].

Chapter 3

Automated CT Segmentation of Diseased Hip Using Hierarchical and Conditional Statistical Shape Models

Abstract

We present a fully automatic method to segment hip joint from CT image with a specific focus on diseased hips, where the fused joint washes out the image features and challenges accurate segmentation. Our approach makes strong use of two types of statistical shape models (SSMs): the hierarchical SSM and conditional SSM. Both SSMs were constructed in the training phase and sequentially applied in the segmentation phase to systematically hone-in on the region of interest, i.e., joint surface, by eliminating other confounders that might otherwise cause erroneous segmentation. Surface subdivisions for the hierarchical and conditional SSM were determined without manual supervision using the canonical correlation analysis that calculates significance of correlation between two points. The proposed framework was evaluated through the segmentation of one hundred female patients (200 hemi-hips) who had underwent total hip arthroplasty. The patients were classified into five disease categories and the hip joints were manually traced by experienced surgeons, which comprised a wellorganized ground-truth dataset for training and testing of the proposed method. Two-fold cross validation studies revealed the average symmetric surface distance of 1.30 ± 0.81 mm for the diseased acetabulum, 1.30 ± 0.72 mm for the diseased femoral head with the proposed method while 1.78 ± 1.61 mm, 1.72 ± 1.00 mm with the conventional method where individual SSM was employed. The proposed method was most effective in severely worn joints, which suggested that the systematic approach effectively decreased the generality and increased specificity in segmentation phase. The accurate segmentation in diseased hips provides quantitative information for quality assurance in treatment planning.

3.1 Introduction

Segmentation of pelvis and femur is critical in an accurate surgical planning and preoperative simulation [4, 21, 22, 5, 23]. Most of the prior work discussed segmentation of healthy hips [24, 25, 26, 27, 28, 29]. No many literature discussed about diseased hips with disease categorization [30]. To our knowledge, this work is only study that validated segmentation of diseased hip categorized on the disease type; however segmentation was not successful in a few portions of the diseased hips. Bone shape abnormality and joint-space narrowing pose a variety of challenges for an automatic segmentation in diseased hips. This thesis addresses the problem of automatic segmentation of diseased hips by efficiently incorporating statistical learning.

Traditional image analysis techniques such as region growing [27], snakes [31], template based method [32, 25], non-rigid registration [28, 33] have been applied in hip segmentation. Graph-cut based interactive method [34] have been applied in mid-foot segmentation. These methods with no prior knowledge tends to produce anatomically implausible shapes in images of diseased hips where there is no or only weak edges apparent at the joint boundary. Statistical shape models (SSMs) [15] have been employed in hip segmentation to incorporate shape prior. Conventional approaches [35, 36] that construct SSM for pelvis and femur individually failed in the region around the joint space due to inconsistency between the two

sSM estimates, which was caused by the erroneous SSM fitting at the weak edges on each side of the boundary. Kainmuller et al. and Schmid et al. [26, 33] utilized the knowledge about the joint kinematics assuming the hip joint as an ideal ball-and-socket joint which is not the case in most of the diseased hip, thus the inaccurate kinematic modeling may lead unexpected error including overlaps of acetabulum and femoral head regions that was solved by the response based method [37] in [33], graph-cut based method [38] in [26]. The two independent studies both reported that segmentation accuracy was lower for the femoral head

than for the acetabulum [26, 33], which led us to hypothesize that the segmentation of femur would become more stable by incorporating knowledge about the stability of segmentation, i.e., constraining the challenging segmentation by using a relatively stable segmentation. In our previous work [12], we utilized joint prior model of the pelvis and femur constructed from combined the pelvis and femur shape. Overlap between the acetabulum and femoral head was solved using hip joint SSM that is combined acetabulum and femoral head SSM. Chandra et al. used combined pelvis and femur SSM with their focused SSM which improved the generality for the acetabulum and femoral head. Combined SSM included relationship between pelvis and femur, but focused SSMs which constructed individually did not include relationship. Furthermore, validation was performed for only healthy hips.

de Bruijne et al. introduced a statistical method in shape prediction for medical image analysis [39]. They proposed a method to predict a vertebral shape based on the conditional SSM of its neighboring bone. Variations of this approach have been applied in the femur [40, 41, 42], and the shoulder [43]. Yang et al. predicted the shoulder shape from the anthropometric, morphometric databases and statistics of the shape of adjacent bones. Statistical prediction methods such as partial least squares (PLS) or conditional SSM were utilized in these works. Although their effectiveness in reconstructing the joint structures was experimentally confirmed, their applications were limited to a validation of the prediction. Albrecht et al. introduced the conditional SSM in the segmentation problem (Albrecht et al., 2013), where some user-supplied anatomical landmarks were used as the condition for segmentation of the femur.

In this thesis, we propose and evaluate a method that achieves an automatic segmentation of the diseased hips by sequentially applying a hierarchical hip SSM and a conditional joint SSM to incorporate increasingly strong shape prior in successive stages. The hierarchical SSM [44] is effective for robust and accurate segmentation. Yokota et al. proposed a hierarchical SSM designed for the hip joint [12], which constitutes a part of the proposed

framework. In the first level of the hierarchy, pelvis and femur are segmented as one object based on the joint distribution of both shapes to put higher priority on specificity over generality for the hip joint shape. In the second and the lower level, pelvis and femur are segmented sequentially using individual pelvis and femur SSMs to prioritize generality over specificity. The conditional SSM is based on the strategy stemmed from the idea that an efficient use of the balance between knowledge from edge features in the image and from statistical learning of the shape would significantly improve robustness and accuracy in the challenging segmentation problem. While the conventional conditional SSM determined the condition surface (i.e., the sub-region that is used as the condition) based on the anatomy features such as the neighboring organs, anatomical region, or manual landmarks (referred to as "anatomy-based" determination), our present work proposes a more statisticallyfounded and consistent way using the canonical correlation analysis (CCA) [45] (referred to as "statistical-based" determination). The proposed method was validated with CT data of 100 patients including 100 diseased hips and 100 unaffected hips (i.e., all patients have a diseased hip on one side and an unaffected hip on the other side) categorized by expert surgeons based on their disease type and severity. The major contributions of this thesis are as follows: (1) a method to systematically determine the order of segmentation of the pelvis and femur by learning from the training dataset, (2) a statistical-based surface sub-division using CCA for construction of the conditional SSM, (3) an extensive validation with a well-organized database which was categorized and ground-truthed by expert surgeons.

The work presented here is algorithmic improvements and enhanced validations of our preliminary works reported in [46]. The algorithmic improvements include the following three aspects. First, while the preliminary work manually determined the order of segmentation based on expert knowledge about the difficulty of the segmentation (i.e., start from the bone that is easier to segment), the present work proposes a systematic strategy to determine the order based on learning from cross-validation tests within the training dataset,

which allows us to extend the same strategy to other population or other anatomies. Second, the conditional SSM was constructed only for the femoral head in the preliminary work, but the acetabulum conditional SSM was added in this study, allowing improvement of the segmentation accuracy. Third, we added a refinement process using the graph-cut as a post-processing to reduce the overfitting error. The enhanced validation includes sensitivity studies to evaluate extensibility of the parameters automatically tuned from the training dataset.

The thesis is outlined as follows. In Section 2, we develop a robust segmentation algorithm specifically targeted at diseased hips. In Section 3 and 4, we illustrate performance of the method using a well-organized patient database consisting of 100 patients (200 hips) classified into 4 disease categories by expert surgeons. A discussion of advantages and limitations of the proposed method, and future works are provided in Section 5. We conclude the thesis in Section 6.

3.2 Materials

CT images of one hundred preoperative female patients of total hip arthroplasty (THA) (i.e., two hundreds hemi-hips) were analyzed in this study. We selected patients who have a diseased hip on one side and a non-diseased hip on the contralateral side (referred to as an "unaffected hip" in this thesis to acknowledge that it was not necessarily healthy but no apparent deformation associated with the disease was identified by an expert surgeon) This way of selecting patients helped analyze the shape variation caused by the disease independent from the anatomical variation. Table 1 shows a list of the disease categories of one hundred diseased hips. We categorized them into two main types. One was a deformed hip (osteoarthrosis of the hip) and the other was collapsed hip (mostly avascular necrosis of the femoral head). The deformed hips are mainly-composed of secondary osteoarthritis, and characteristic tendency of the disease progression was displayed in their shape deformation.

Table 3.1: Number of cases in each disease category.

Category of disease			Number of cases
	Primary osteoar	7	
Deformed hip	Secondary osteoarthritis	Crowe 1	58
		Crowe 2, 3, 4	24
	Avascular necrosis of the femoral head		10
Collapsed hip	Rapidly destructive co.	1	

Table 3.2: Specification of the CT scanning.

Vertical extent	From the top of the pelvis to the distal end of the femur
FOV	$360 \times 360 \text{ mm}$
Matrix size	$512 \times 512 \ \mathrm{mm}$
Slice thickness (pelvis to proximal femoral shaft)	2.0 mm

There were twenty 24 cases that were severer than crowe grade 2, which exhibited severe deformation both in acetabulum and femoral head. In the class of collapsed hips, deformation is generally limited to the bone tissue and the cartilage tends to be relatively intact, which makes the bone edges more distinct. Figure 1 shows the axial, coronal slices and the 3D surface rendering of CT data of five representative cases. The unaffected hip presents clear boundary between the pelvis and femur, while the deformed hips exhibit deformation at the acetabulum and femoral head, lose the cartilages, and thus lack the edge information around the joint boundary.

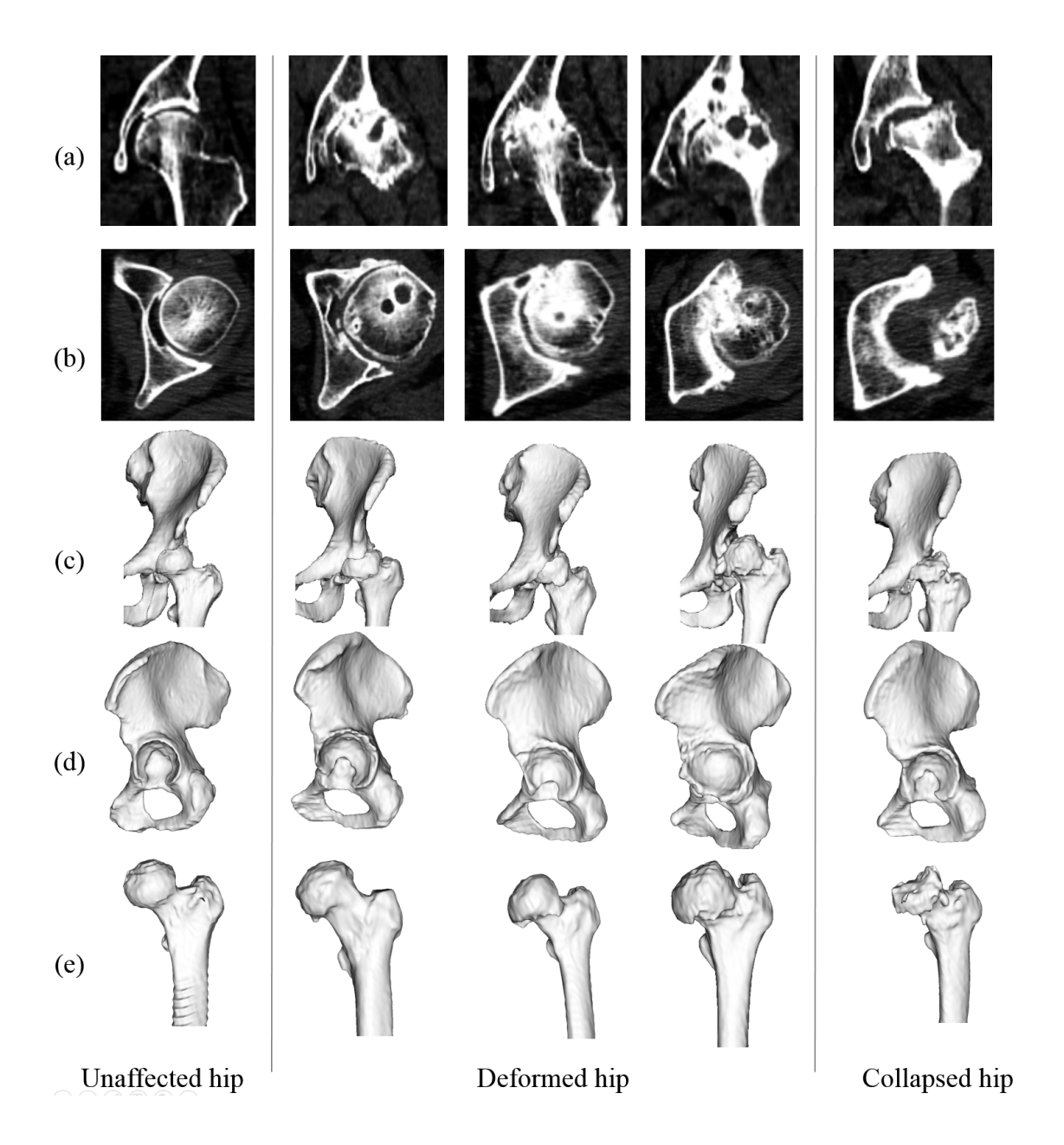


Figure 3.1: CT images of the representative cases. (a) and (b) Coronal and axial slices. The window and level for all images are 800 and 400 HU. (c), (d) and (e) 3D renderings of the hip, pelvis and femur.

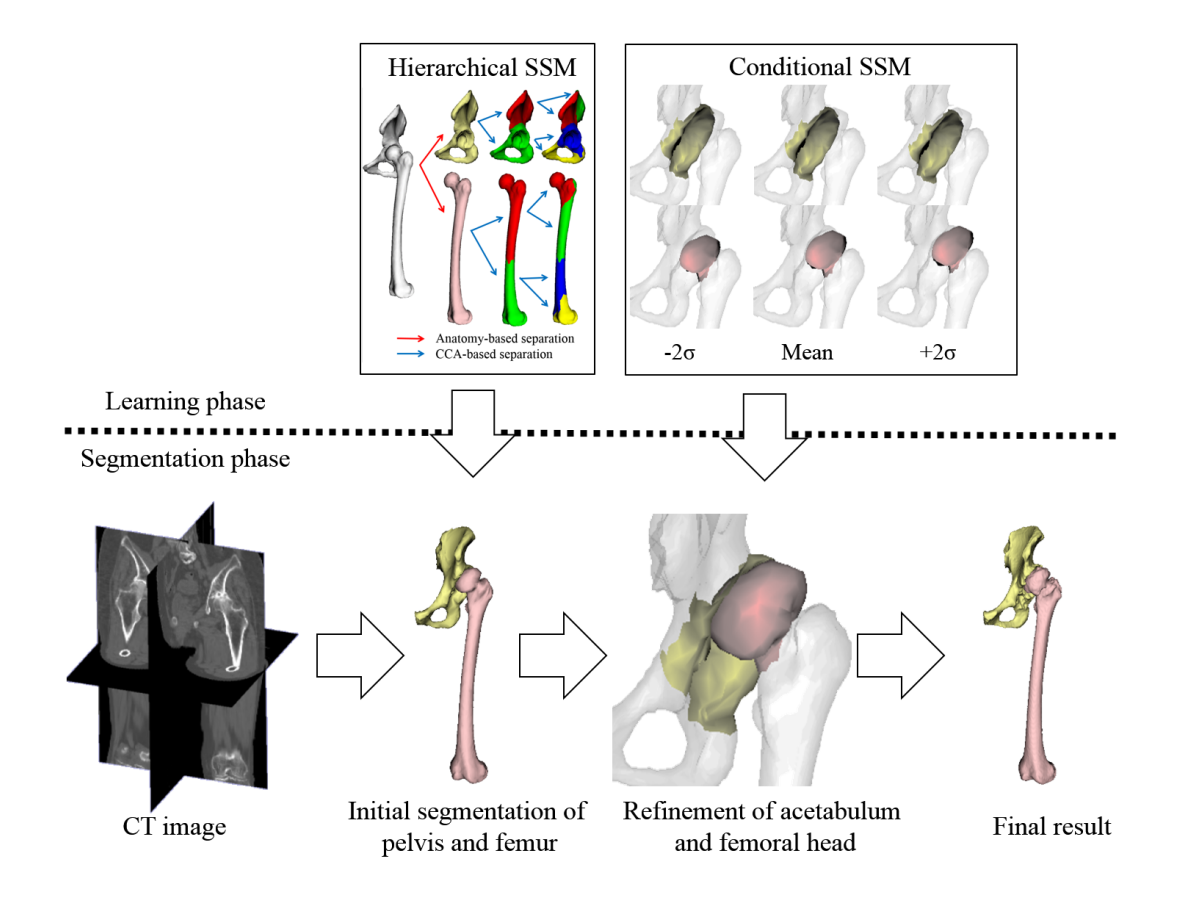


Figure 3.2: Overview of proposed method.

3.3 Methods

3.3.1 Overview of the proposed framework

There are two phases in the proposed framework: learning phase and segmentation phase (Fig. 3.2). The training phase constructs two types of SSM: a hierarchical SSM of the hip (detailed in section 3.3.1) and conditional SSMs of the acetabulum (A-SSM) and the femur head (FH-SSM) (detailed in section 3.3.2). The segmentation phase first normalize the pelvis coordinate system using automatically localized landmarks (detailed in section 3.2), then segments the entire bone regions using the hierarchical hip SSM (section 3.4.1) and refines the joint boundary using the conditional A-SSM and FH-SSM (section 3.4.2).

We hypothesized that the proposed multi-phase strategy is effective to gradually increase constraint by the prior knowledge as stability of the segmentation decreases due to obscure boundaries. The strategy utilizes a mild constraint by the pelvis-femur combined SSM in the first stage when the target edge boundary (i.e., boundary between bone and soft tissue) is clear, whereas a stronger constraint by the conditional SSMs is used in later stage when the CT value provides very little information of the boundary due to degeneration of the joint.

3.3.2 Localization of pelvic anatomical landmarks using statistical learning

Anatomical landmarks on the pelvis in each subject CT were automatically localized using a previously reported method [47], which consists of the following three steps:

- 1. Spatial normalization and cropping of ROI using the probabilistic atlas
- 2. Localization of anatomical landmarks using the statistical landmark model
- 3. Refinement of the pelvic anatomical coordinate using the average symphysial surface image

The localized landmarks were used in both model construction and segmentation to obtain an initialization for the segmentation.

3.3.3 Learning phase

Construction of the hierarchical hip SSM

The previous method optimized the shape parameters of all sub-regions simultaneously, where all the sub-regions were treated equally, which degraded segmentation accuracy since the boundary determination became unstable in the region where the apparent image features

were significantly weak such as the diseased hip joint. Therefore, in this thesis, we chose a sequential approach to avoid this ambiguity in determination of the boundary. The edge search in segmentation of a latter object ignores the region that was labeled in the earlier segmentation. The order of the optimization was automatically determined using the training dataset as detailed later.

Fig. 3 illustrate the proposed hierarchical hip SSM. The top level in the hierarchy was an SSM of the entire hip joint combining pelvis and femur, the second level was individual SSMs of pelvis and femur, and the third and lower level are SSMs of sub-regions of the pelvis and the femur, where the sub-regions were automatically determined by canonical-correlation analysis (CCA).

A p-value to test the correlation between two points is derived using CCA [45] to find intra-organ relations in surface S. Note that we have multiple surfaces in the training dataset and correspondence of all vertices have already been established. Thus, the CCA deals with a point on all surface meshes as a set (i.e., if there are N subjects, one point was represented as a 3N element vector and correlation between two 3N vectors were computed with CCA). First, a pair of points on the target surface S, denoted by $\{x, y\}$, having the highest p-value (i.e., lowest correlation) in all combinations of vertices on S was selected.

$$\{\hat{x}, \hat{y}\} = \operatorname*{argmax}_{x \in S, y \in S} p(x, y) \tag{3.1}$$

A set of points on S whose p-value with \hat{x} was smaller than that with \hat{y} (i.e., points with higher correlation with \hat{x}) was defined as one sub-region S_x , and the other points are defined as the other sub-region S_y .

$$S_x = \{ s \in S \mid p(\hat{x}, s) \le p(\hat{y}, s) \}$$

$$S_y = \{ s \in S \mid p(\hat{x}, s) < p(\hat{y}, s) \}$$
(3.2)

Each SSM was constructed in a standard framework where the principal component analysis was applied to vectors representing x, y, z coordinate of all vertices on a surface of all

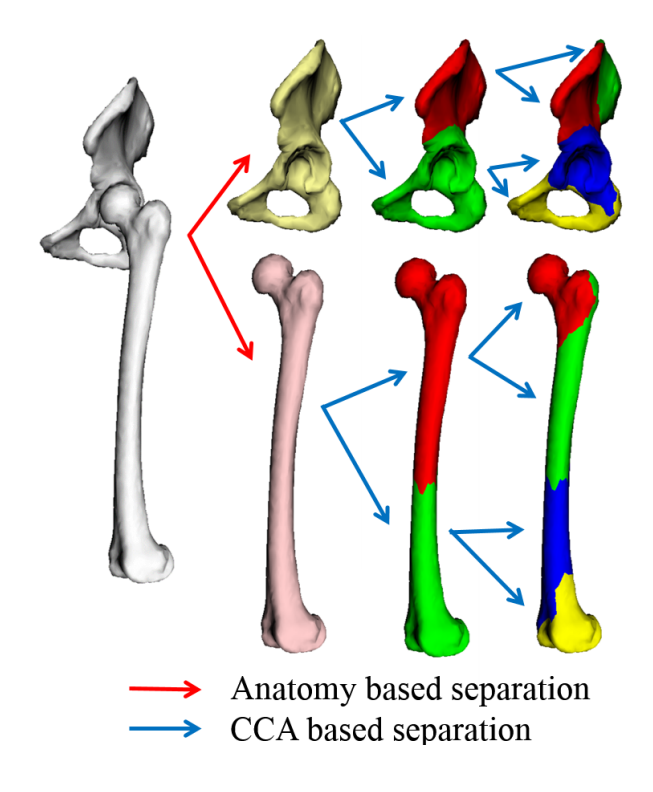


Figure 3.3: Hierarchical hip SSM. Anatomy-based separation is performed in second level. CCA-based separation is performed in third or lower level.

training datasets [48].

$$\mathbf{q}_{hi}(\mathbf{b}_{hi}) = \bar{\mathbf{q}}_{hi} + \mathbf{\Phi}_{hi}\mathbf{b}_{hi} \qquad (i = 1, \dots, N_h)$$
(3.3)

To establish correspondence between vertices of the training surface, we employed the pairwise registration approach [49] using a template subject selected from the training dataset. The template selection is detailed in Appendix. The registration used the free-form deformation based method [50].

The order of the sequential segmentation in the second level of the hierarchy using the individual femur and pelvis SSM was determined in a way such that the leave-one-out cross valid.

Construction of conditional A-SSM and FH-SSM

First, we determined the acetabulum and femoral head region for which the conditional SSM is constructed in the following automatic manner. We defined the p-value of a point x with the surface Y as follows,

$$p(x,Y) = \inf\{p(x,y) \mid y \in Y\}$$
 (3.4)

A set of points on a surface X whose p-value with the surface Y is lower than a predefined threshold T is defined as a sub-region X'.

$$X' = \{ x \in X \mid p(x, Y) < T \}$$
(3.5)

The threshold T was tuned with the training dataset as shown in the result section.

The conditional A-SSM was constructed as an SSM of the acetabulum region conditioned on the region except the acetabulum. The same method was applied to the femoral head regions to construct the conditional FH-SSM. The conditional probability distribution of a shape X given a sub-region segmented in the previous step Y_0 can be represented as

$$P(X \mid Y = Y_0) = N(\mu_{X|Y_0}, \Sigma_{X|Y_0})$$
(3.6)

$$\mu_{X|Y_0} = \mu_X + \Sigma_{XY} \Sigma_{YY}^{-1} (Y_0 - \mu_Y)$$
(3.7)

$$\Sigma_{X|Y} = \Sigma_{XX} - \Sigma_{XY} \Sigma_{YY}^{-1} \Sigma_{YX}$$
(3.8)

where μ_X and μ_Y are the average of X and Y in the training dataset. Σ_{XX} , Σ_{XY} , Σ_{YX} , Σ_{YY} are the joint covariance matrix defined as follows,

$$\Sigma = \begin{bmatrix} \Sigma_{XX} & \Sigma_{XY} \\ \Sigma_{YX} & \Sigma_{YY} \end{bmatrix} = \begin{bmatrix} Cov(X,Y) & Cov(X,Y) \\ Cov(Y,X) & Cov(Y,Y) \end{bmatrix}$$
(3.9)

Ridge regression is used to calculate Σ_{YY}^{-1} , i.e. Σ_{YY}^{-1} is replaced by $(\Sigma_Y Y + \gamma I)^{-1}$. Fig. 4 presents constructed conditional SSMs of the acetabulum and femoral head. The average shape and model deformation of the standard SSM are constant with patients, whereas the average shape fits the patient-specific shape and the model deformation is restricted.

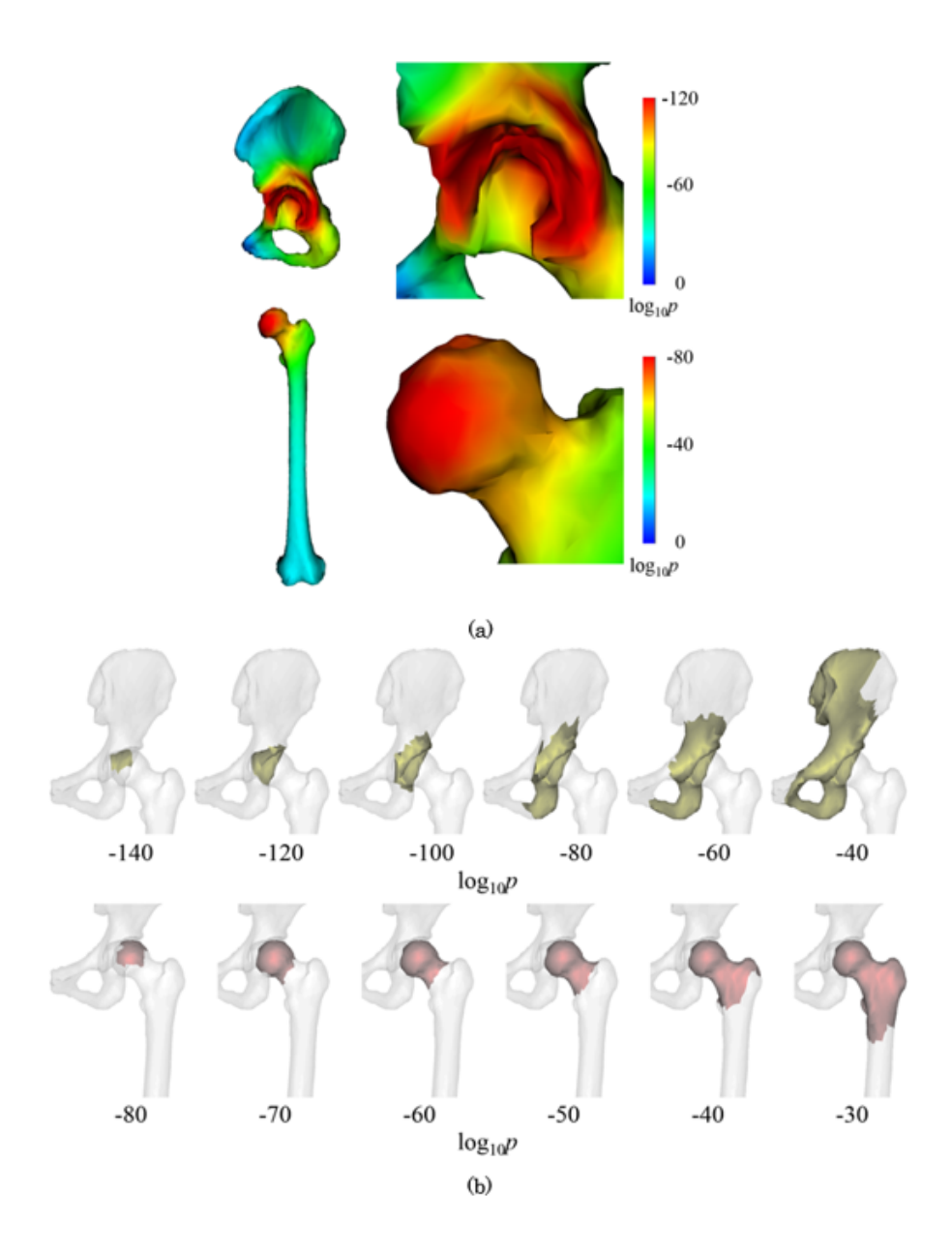


Figure 3.4: The extent of sub-region representing the acetabulum and femoral head determined by CCA. (a) p-value map on the basis of CCA of the femur surface influenced by the pelvis and the pelvis surface influenced by the femur. Smaller values indicate stronger correlation with the adjacent bone. (b) The acetabulum and femoral head region obtained by the corresponding p-value threshold.

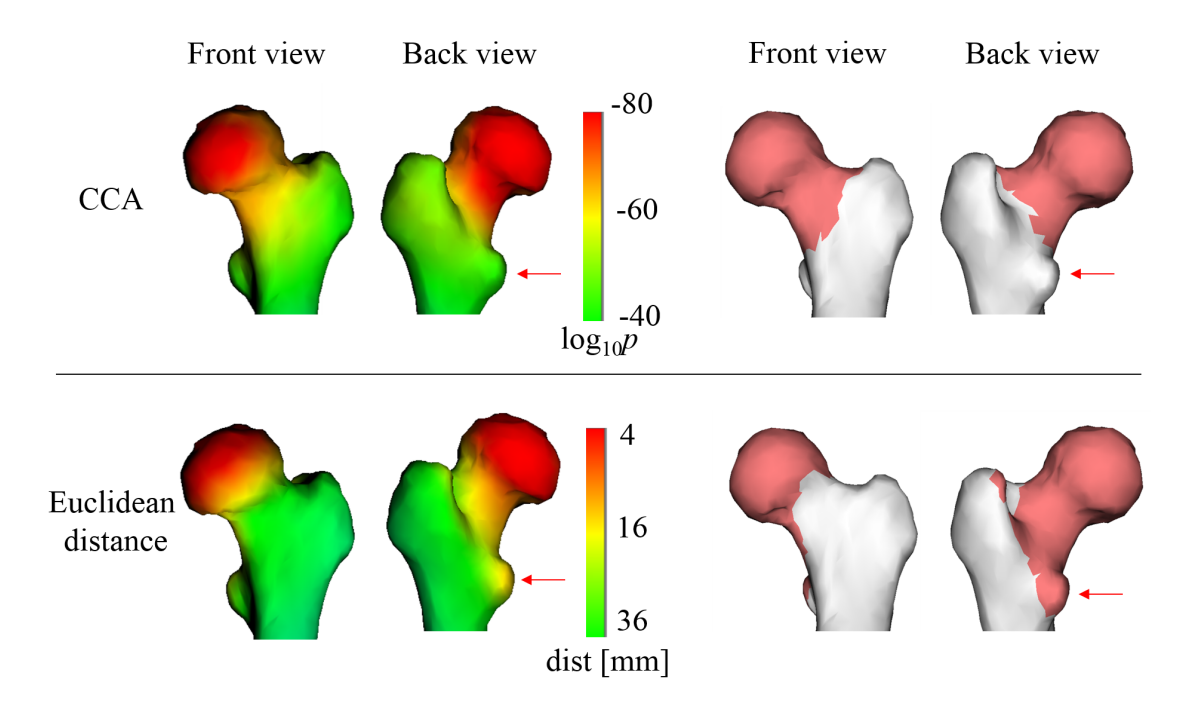


Figure 3.5: The extent of sub-region representing the acetabulum and femoral head determined by CCA. (a) p-value map on the basis of CCA of the femur surface influenced by the pelvis and the pelvis surface influenced by the femur. Smaller values indicate stronger correlation with the adjacent bone. (b) The acetabulum and femoral head region obtained by the corresponding p-value threshold.

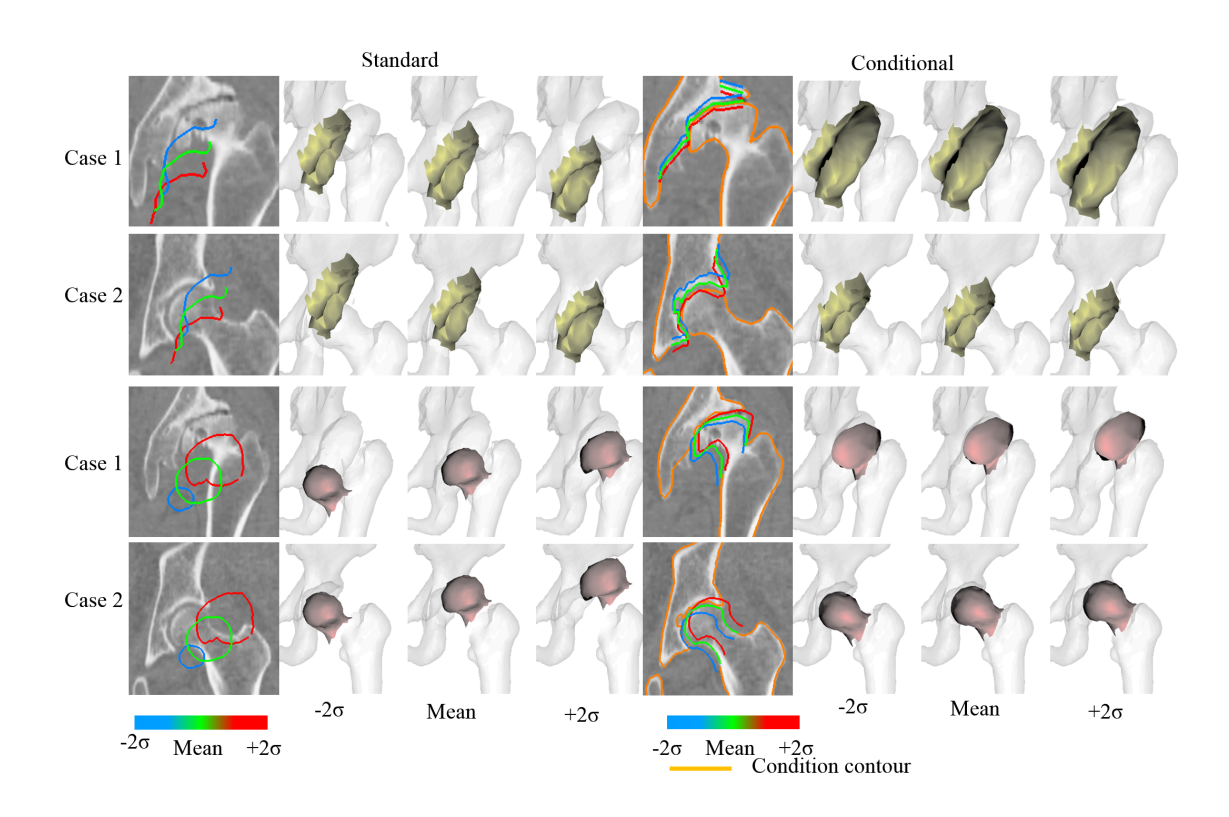


Figure 3.6: The first mode of the standard and conditional FH-SSM and A-SSM. The upper two rows show SSMs of the acetabulum for two different patients (referred to as case 1 and case2), while the lower two rows are the femoral head. In each case, a coronal slice overlaid with contour lines of $+2\sigma$, mean, and -2σ surfaces is shown at the left column and the other three columns show 3D visualization of each surface. The standard SSMs are the same for both cases, since there is no constraint from segmentation of the other bone. Conditional SSMs for both cases are change by target contour.

3.4 Segmentation phase

The segmentation phase includes the following steps

- 1. Automatic localization of the pelvis coordinate system (detailed in section 3.2)
- 2. Initial rough segmentation of the bone region by thresholding
- 3. Segmentation using the hierarchical hip SSM
- Refinement of acetabulum and femoral head using the conditional A-SSM and FH-SSM
- 5. Refinement using the graph-cut

In step (2), the largest connected component was extracted. The threshold was automatically learned from the cross-validation within the training dataset.

Hierarchical hip SSM segmentation

The segmentation using the hierarchical hip SSM is summarized in algorithm 1.

Fitting of the SSM to a point cloud was performed with the Levenberg-Marquardt method using the following cost function as in [51, 52].

$$\hat{\mathbf{b}} = \underset{\mathbf{b}}{\operatorname{argmin}} \left(\frac{1}{N_E} \sum_{x \in E} D(x, S(\mathbf{b})) + \frac{1}{N_q} \sum_{x \in S(\mathbf{b})} D(x, E) + \frac{\lambda}{M} ||\mathbf{b}||^2 \right)$$
(3.10)

where b is a shape parameter vector, $S(\mathbf{b})$ is a shape instance defined by the parameter b, E is a cloud of edge points, N_E is the number of edge points, N_q is the number of vertices in $S(\mathbf{b})$, D is a distance metric, M is number of modes. The first two terms represents fitness between a shape instance and the detected edge points and the last term represents a penalty to avoid a shape far from the mean.

Algorithm 1 Segmentation using hierarchical hip SSM (HH-SSM)

N = number of hierarchical levels

 $HH - SSM_1 =$ combined pelvis and femur SSM

 $HH - SSM_2 =$ individual pelvis and femur SSMs

 $HH - SSM_3, \dots, N =$ pelvis and femur sub-region SSMs

E0 = Initial edge points (computed by thresholding)

S1 = A surface instance of HH-SSM1 fitted to E0

for n=1 to N do

En = Edge points searched in the image initialized by Sn

 $S_{n+1} = A$ surface instance of HH-SSMn fitted to En

end for

In this thesis, we use the same notation, D(x, A), for two similar distance metrics: point-to-surface-mesh distance and point-to-point-cloud distance. Both metrics measure the shortest distance between and A as follows,

$$D(x, A) = \inf\{||x - p||^2 \mid p \in A\}$$
(3.11)

That is, D(x, A) indicates the shortest distance between x and elements in A. If the right argument A is a surface mesh such as a shape instance derived from an SSM as in the first term in eq(10), $p \in A$ indicates any point on the surface mesh including a point in-between vertices (i.e., any point on a triangle consisting of connected three vertices). If A is a point cloud as in the second term, $p \in A$ simply indicates a point in the point cloud. The second term, distance from vertices in the shape instance to edge points, was ignored in the first level to avoid an erroneous fitting due to the outlier edge points that are significantly far from the target region such as the edge of the sacrum.

The edge search in the algorithm 1 used an intensity profile around the boundary of the shape instance computed by the shape parameters and searched edge points based on a threshold which we learn from the training dataset as detailed in the result section.

[48] proposed an additional penalty term called adhesiveness constraint which penalized the distance between vertices around the edge of the neighboring regions to keep continuity of the surface at the border. However, [52] suggested that the constraint did not add significant improvement, thus we did not employ it.

Refinement of acetabulum and femoral head using the conditional A-SSM and FH-SSM

The segmentation obtained in the previous stage was refined by the conditional A-SSM and FH-SSM as follows.

- Compute a sub-region in acetabulum and femoral head that is used as the condition (referred to as condition surface)
- 2. Construct the conditional SSM using the condition surface
- 3. Perform segmentation using the conditional SSM

The order of the segmentation was determined by cross-validation within the training dataset in the same way as the learning phase (see 3.3.1). The edge search in this stage searched only those voxels which were not included in the region already segmented.

Refinement using the graph-cut

Further refinement was performed using the graph-cut [53]. We defined the energy term as

$$B_{p,q} = exp\left(-\frac{(I(p) - I(q))^2}{2\sigma^2}\right) \cdot \frac{1}{||p - q||^2}$$
(3.12)

Where σ was the variance in intensity of the neighboring voxels computed by

$$\sigma = \sqrt{\frac{1}{N_p - 1} \sum_{p \in R} \sum_{q \in N(p) \cap R} (I(q) - I(p))^2}$$
 (3.13)

In this thesis, the hard constraint regions for object and background are automatically determined based on segmented region R. Let $H_{R(I)}$ be probability distribution of intensity histogram within R. The hard constraint regions for object and background O and B are defined as

$$O = \{ p \mid p \in R, H_{R(I(p))} \ge t(p_O; H_R) \}$$
(3.14)

$$B = \{ p \mid p \in \bar{R}, H_{R(I(p))} \le t(p_B; H_R) \}$$
(3.15)

where $t(p; H_R) = min\{t \mid \Sigma_{j \in J(t; H_R)} H_{R(I=j)} \geq p\}$ is p-percentile value of H_R , p_O and p_B are percentile values to determine the hard constraint regions for object and background, respectively.

The graph edges were not created between the nodes at the joint boundary in order to keep the segmentation by the conditional SSM in the previous step. Thus, overlaps between the pelvis and femur regions does not occur.

3.5 Results

3.5.1 Experimental conditions

Two-fold cross validations were conducted. The 200 CT data of the hips (100 patients) were randomly divided into two groups and the proposed algorithm was tested on one group using the other group as a training dataset. The two-fold cross validation was performed five times using different combination of the training dataset and the average error was evaluated.

Three methods listed below were performed for the comparative study.

 Individual SSM: The pelvis and femur SSMs were constructed individually. Thus, this model was not include the relationships between the pelvis and femur. The order of segmentation and removal the regional overlaps between the pelvis and femur were same as the proposed method. The femoral anatomical landmarks (the lesser trochanter, condyles medialis, condyles lateralis, gluteal tuberosity) were manually localized, because the individual femur SSM require these landmarks to perform the spatial normalization.

- 2. Hierarchical SSM: The hierarchical hip SSM (see Section 3.4.1).
- Hierarchical and conditional SSM (proposed method): Segmentation with the conditional SSM was performed after the segmentation with the hierarchical SSM (see Section 3.4.2).

Since the Hierarchical SSM and the Hierarchical and Conditional SSM intrinsically includes estimation of the pose of the femur, these methods did not require the manual localization of the femoral anatomical landmarks as opposed to the individual SSM.

Manual trace was used as the ground truth. These traces were verified by experienced orthopaedic surgeons. For the purpose of performance evaluation described below, the error metric was computed only on the part of the pelvis and femur, i.e., acetabulum and femoral head regions, because the are the most critical in decision making in the hip surgery.

The average symmetric surface distance (ASD) [54] was used as the error metric throughout the experiment. Metrics that quantify overlap between two regions, such as Jaccard and Dice indices, were not computed because the ground truth in this study was not a labeled region but an open contour.

Extraction of surface vertices from a labeled volume was performed by the marching cubes algorithm followed by decimation using Visualization Toolkit (VTK). Then Image Registration Toolkit (version 2.0) was used to establish correspondence of the vertices [55]. The algorithm was implemented in C++ on a workstation with 3 GHz CPU and 12 GB RAM.

3.5.2 Experimental results

Parameter tuning via the leave-one out cross validation with the training dataset

Fig. 5 and Fig. 6 illustrate results of the tuning step for threshold value used in the first and second level of hierarchical SSM. The threshold of 175 HU for the hip (combined the pelvis and femur), 225 HU for the acetabulum and 125 HU for the femoral head achieved the lowest ASD in all five two-fold cross validation tests, thus we employed these values in the experiment below.

ASD at the acetabulum surface and the femoral head were 1.32 mm and 3.46 mm, respectively, in the leave-one-out test used the pelvis and femur SSMs individually, indicating that the segmentation provides better accuracy on the acetabulum surface than on the femoral head. Therefore, sequential approach was performed, i.e. the segmentation of the femur was performed after the pelvis. Then, ASD at the femoral head was improved to 0.89 mm.

Fig. 7 shows the determination of the extent of sub-region representing the acetabulum and femoral head determined by CCA. The region which has strong correlation with adjacent bone was colored in red, while blue region indicated weaker correlation. Strong correlation appeared near the acetabulum and femoral head as expected. The tendency that p-value for the pelvis was lower than that of the femur was confirmed. The correlation was different even if two bones were adjoined. This results caused by large variety of the femoral pose whereas no variety of the pelvic pose using special normalization.

Fig. 8 shows the effects thresholding of p-value in determination of the extent of the acetabulum and femoral head using CCA and γ in ridge regression. The extent narrowed with decrease in threshold for p-value. Shape variation was restricted with decrease in γ . These two parameter were tuned simultaneously. When $log_{10}p = -100$ and $log_{10}\gamma = -1$ for the acetabulum, ASD reached 0.98 mm. When $log_{10}p = -70$ and $log_{10}\gamma = -1$ for the femoral head, ASD reached 0.99 mm. Thus, the acetabulum was performed before the femoral head.

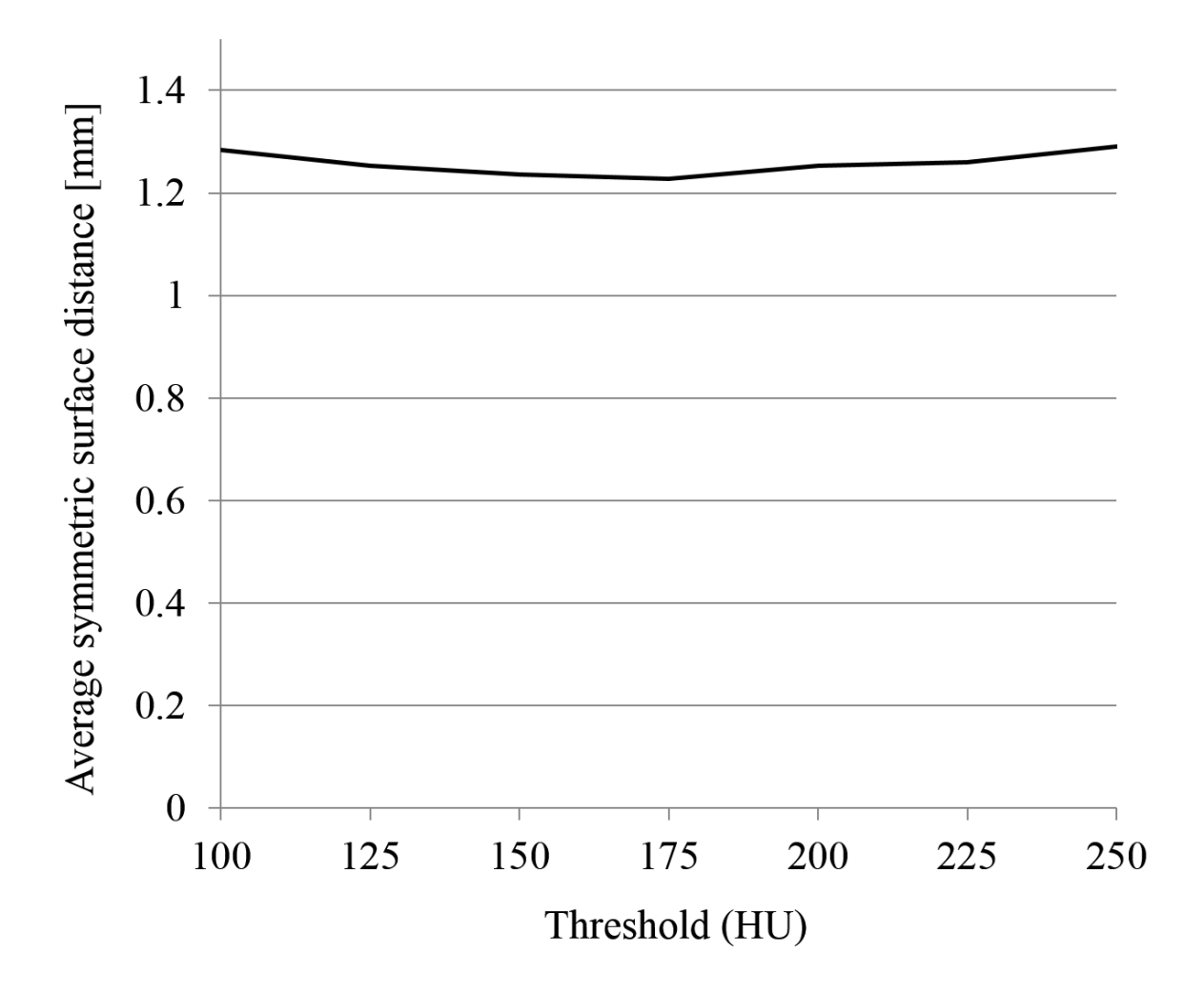


Figure 3.7: Dependency of the threshold value on ASD in the hip bone that was used for tuning of the threshold value in the first level of hierarchical SSM.

 $log_{10}\gamma=-1$ was optimal value in any threshold for p-value. Thus, it could find the optimal parameters with individual optimization, rather than with simultaneous optimization. In other words, optimal γ was calculated firstly and then optimal threshold for p-value was calculated.

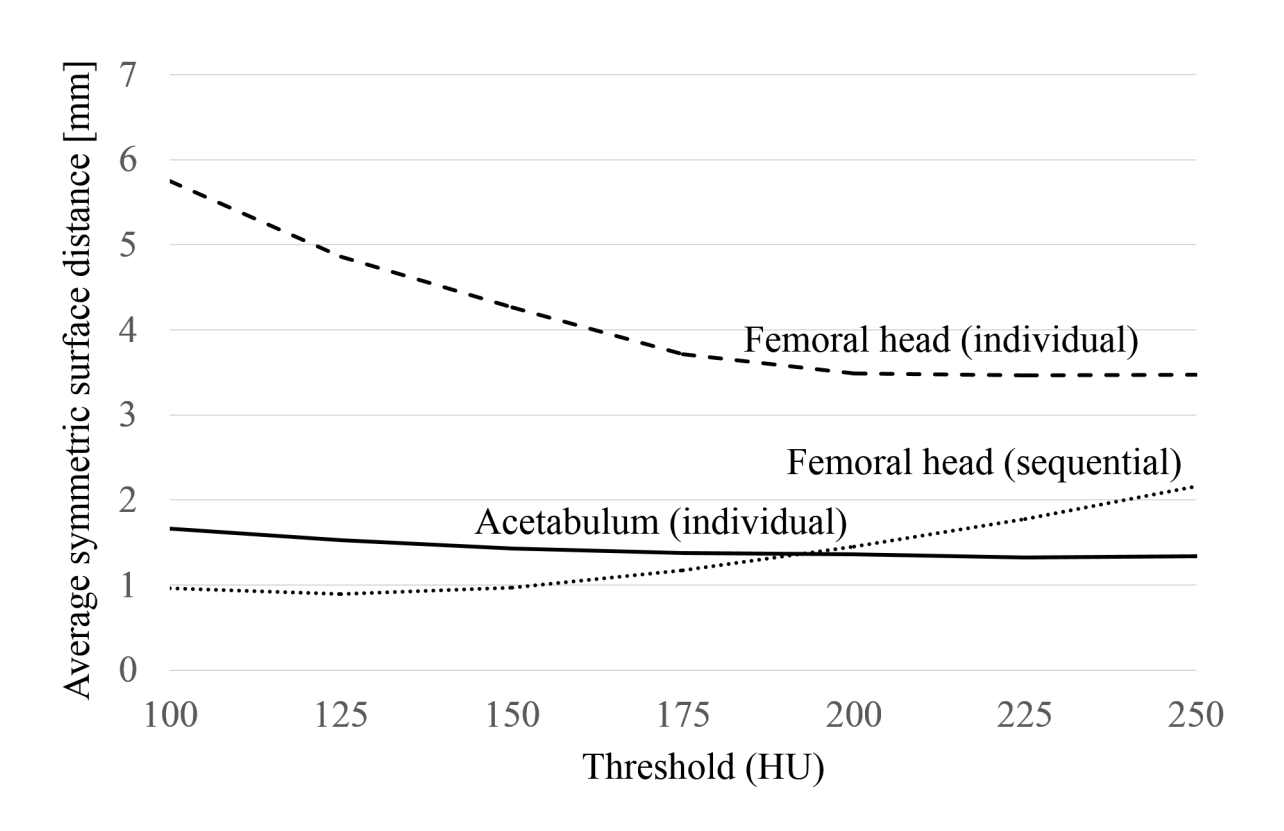


Figure 3.8: Dependency of the threshold value on ASD in the acetabulum and femoral head that was used for tuning of the threshold value in the second level of hierarchical SSM.

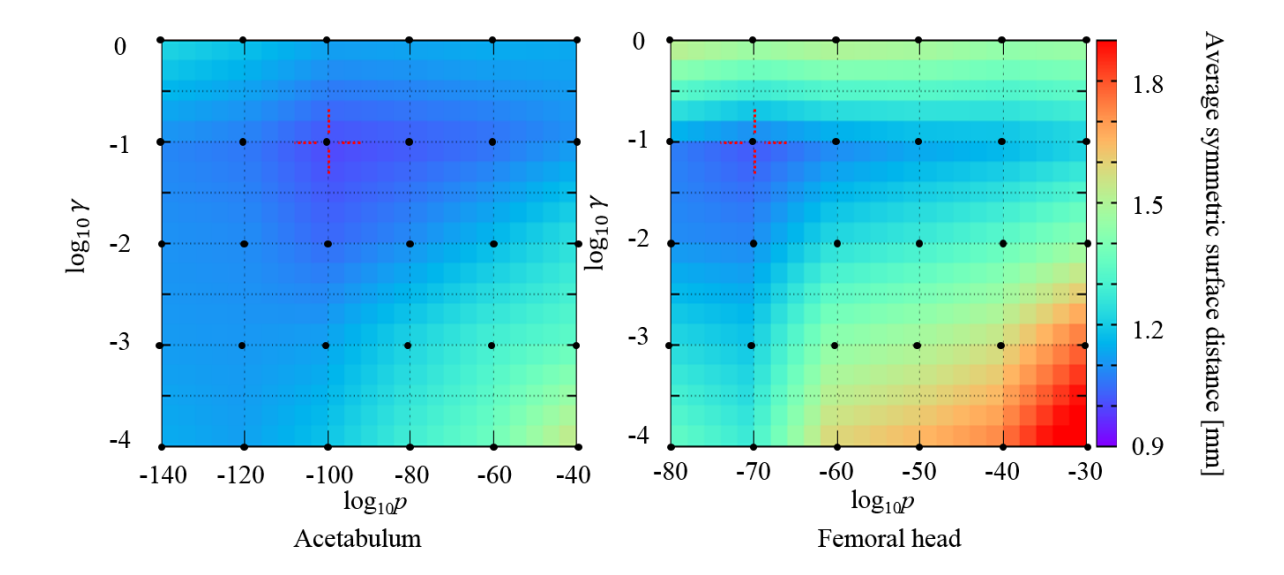


Figure 3.9: ASD as a function of the two parameters: p-value in determination of the condition surface using CCA and γ in ridge regression. The dotted points are the sample points at which the ASD values were actually computed and the colormap shows linear interpolation between the sample points. The dashed red lines indicate the minimum value.

Performance comparison between diseased and unaffected hips

Figure 9 and Table 3 present the comparison of the segmentation accuracy between unaffected hips and diseased hips. For the acetabulum of unaffected hips, both methods exhibited comparable accuracy. For the femoral head of unaffected hips, the proposed method produced significant improvement compared with the hierarchical SSM (p < 0.01). For the acetabulum and femoral head of diseased hips, proposed method and hierarchical SSM produced significant improvement compared with the individual SSMs (p < 0.01).

Table 3.3: Evaluation results for segmentation accuracy of diseased and unaffected hips. Mean and standard deviation of ASDs [mm] are shown in each method. The best results are shown in a bold font.

	Acetabulum		Femoral head	
	Unaffected	Diseased	Unaffected	Diseased
Individual SSM	0.77±0.38	1.78±1.61	1.33±1.27	1.72±1.00
Hierarchical SSM	0.73±0.19	1.33±0.85	1.11±0.64	1.31±0.83
Hierarchical and conditional SSM (Proposed method)	0.72±0.18	1.30±0.81	0.90±0.43	1.30±0.72

Performance comparison between types of disease

Figure 10 and Table 4 demonstrate the comparison of the segmentation accuracy between disease categories. By employing the proposed method, significant improvements were achieved in all categories. The proposed method especially produced considerable improvement especially for crowe grade 2, 3 or 4. For collapsed hips, even though the edge at the joint was clear, segmentation failed most likely due to the lack of training dataset which is discussed later.

Performance for whole pelvis and femur

Table 5 shows the accuracy evaluation results for the whole pelvis and femur. There were no significance for each methods. The reason being that segmentation errors at other joints (e.g. the knee or sacrum) were larger than the hip joint because of no prior for these joints. Moreover, the regions of the acetabulum and femoral head were considerably smaller than that of the whole pelvis and femur.

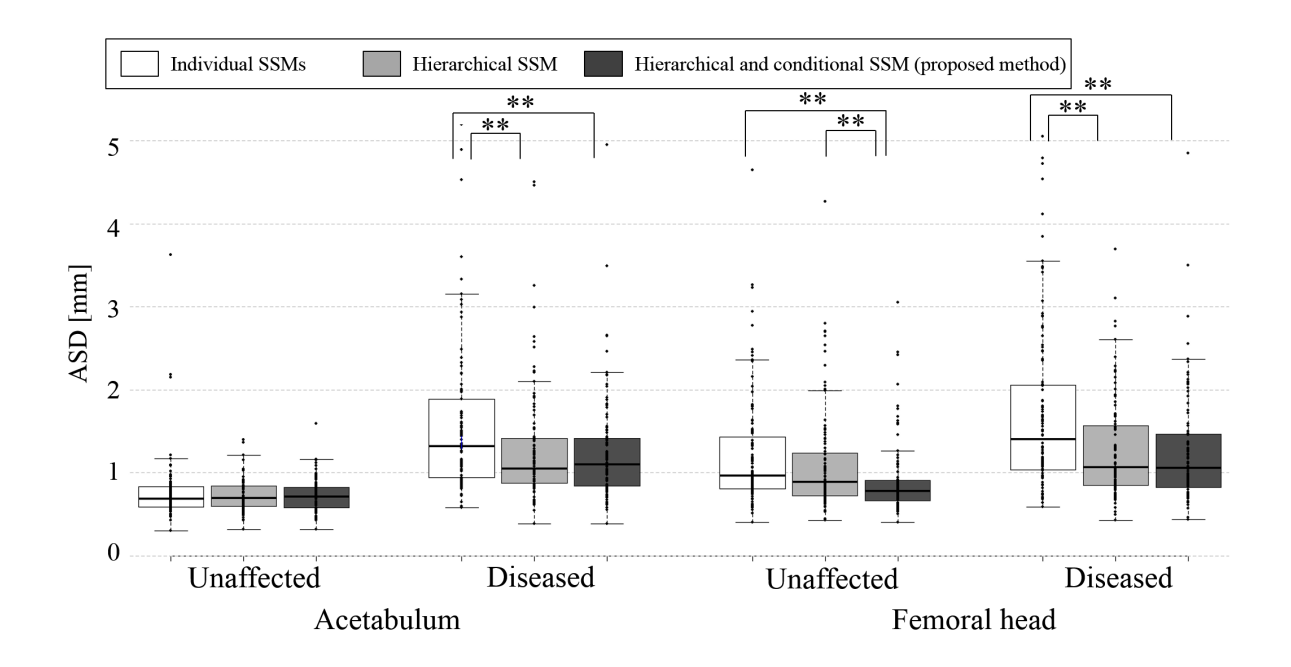


Figure 3.10: Boxplots showing segmentation accuracy of diseased and unaffected hips. * and **: significant improvement; *: 0.01 , **: <math>p < 0.01.

Representative results of each method

Fig. 11 illustrates coronal views and 3D renderings of four representative cases. The advantage of the proposed hierarchical and conditional SSM against the individual SSM was clearly confirmed from the consistency between the acetabulum and femoral head boundaries (case1, 2 and 3). The proposed method could segmented properly for these cases, even though the edge information at the joint was insufficient. In spite of significant improvement for the collapsed hips using the proposed method, segmentation failure in the collapsed hip was confirmed for the case 4, though the boundary was clear. Fig. 12 demonstrates the worst case by the proposed method in terms of ASD.

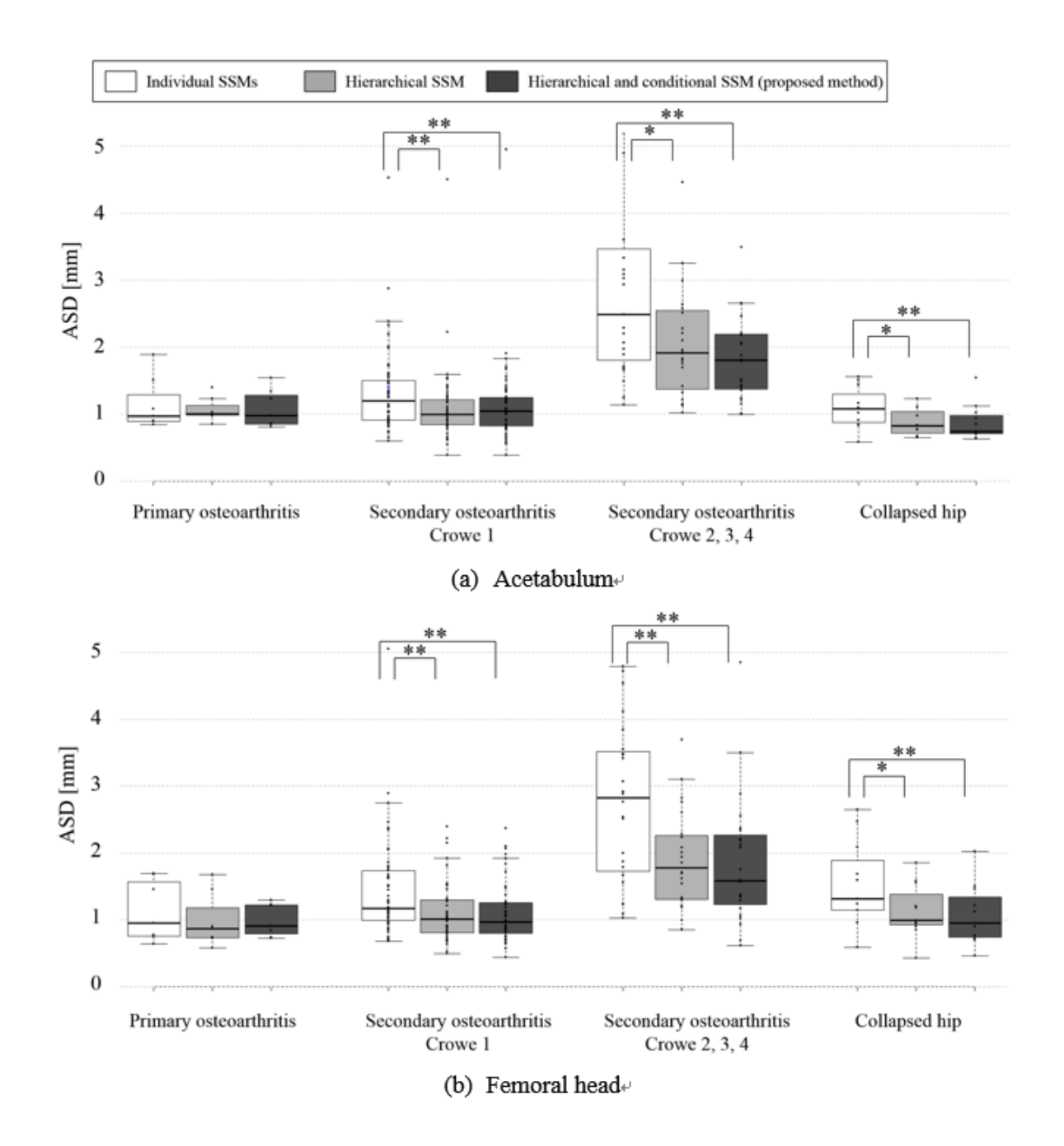


Figure 3.11: Boxplots showing segmentation accuracy for each disease category in the acetabulum and femora head. * and **: significant improvement; *: 0.01 , **: <math>p < 0.01.

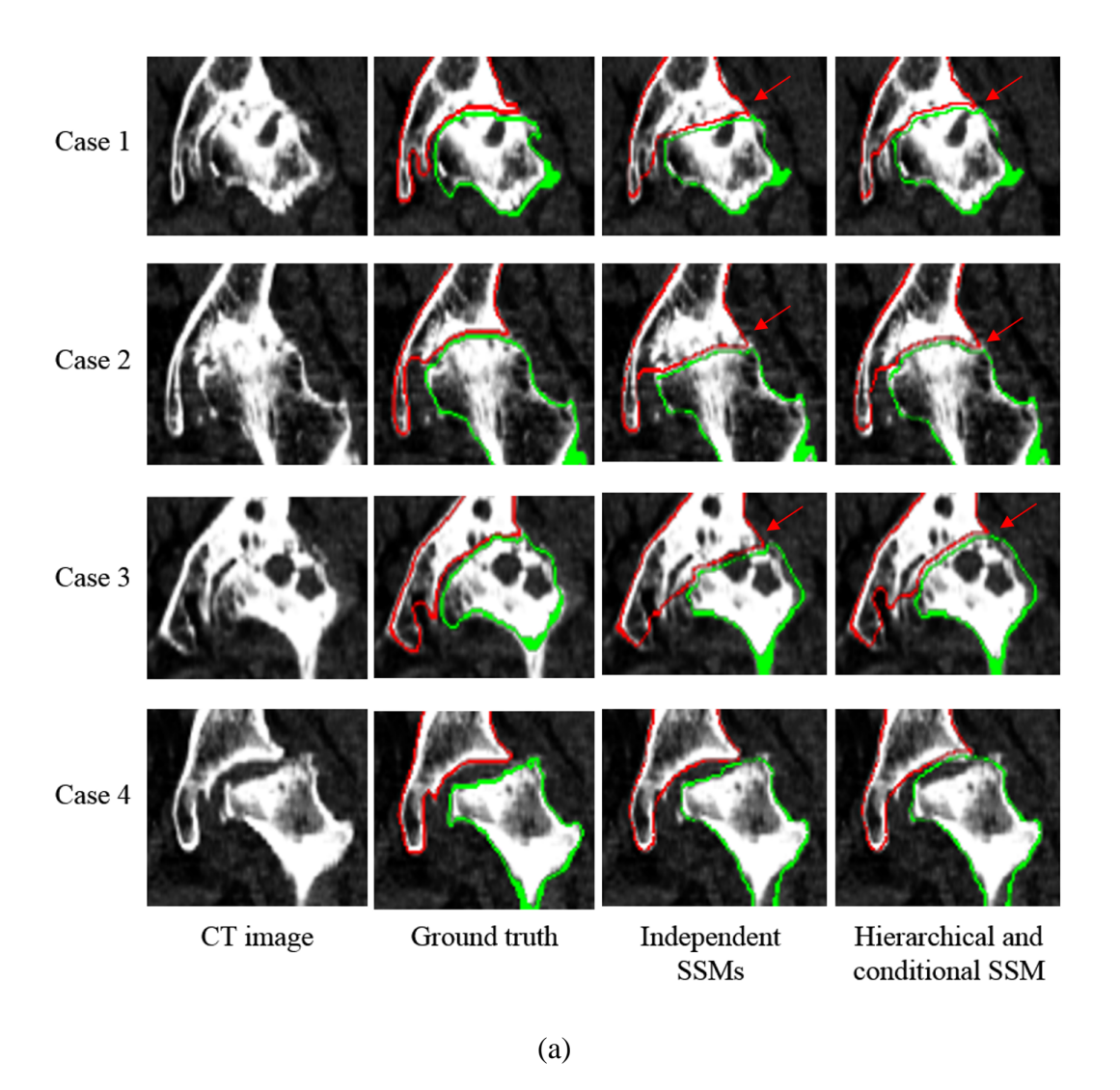


Figure 3.12: Segmentation results of the representative case of each disease category. Case 1, 2, 3, and 4 correspond to osteoarthritis, crowe 1, crowe 2 and collapsed hip, respectively. (a) coronal slices at the plane of the approximate femoral center. The green and red contours correspond to the segmented regions of the pelvis and femur, respectively. Arrows in (a) indicate the part where segmentation accuracy improved with the hierarchical and conditional SSM. (b) and (c) 3D rendering of the segmented surface with colormap indicating the surface distance error.

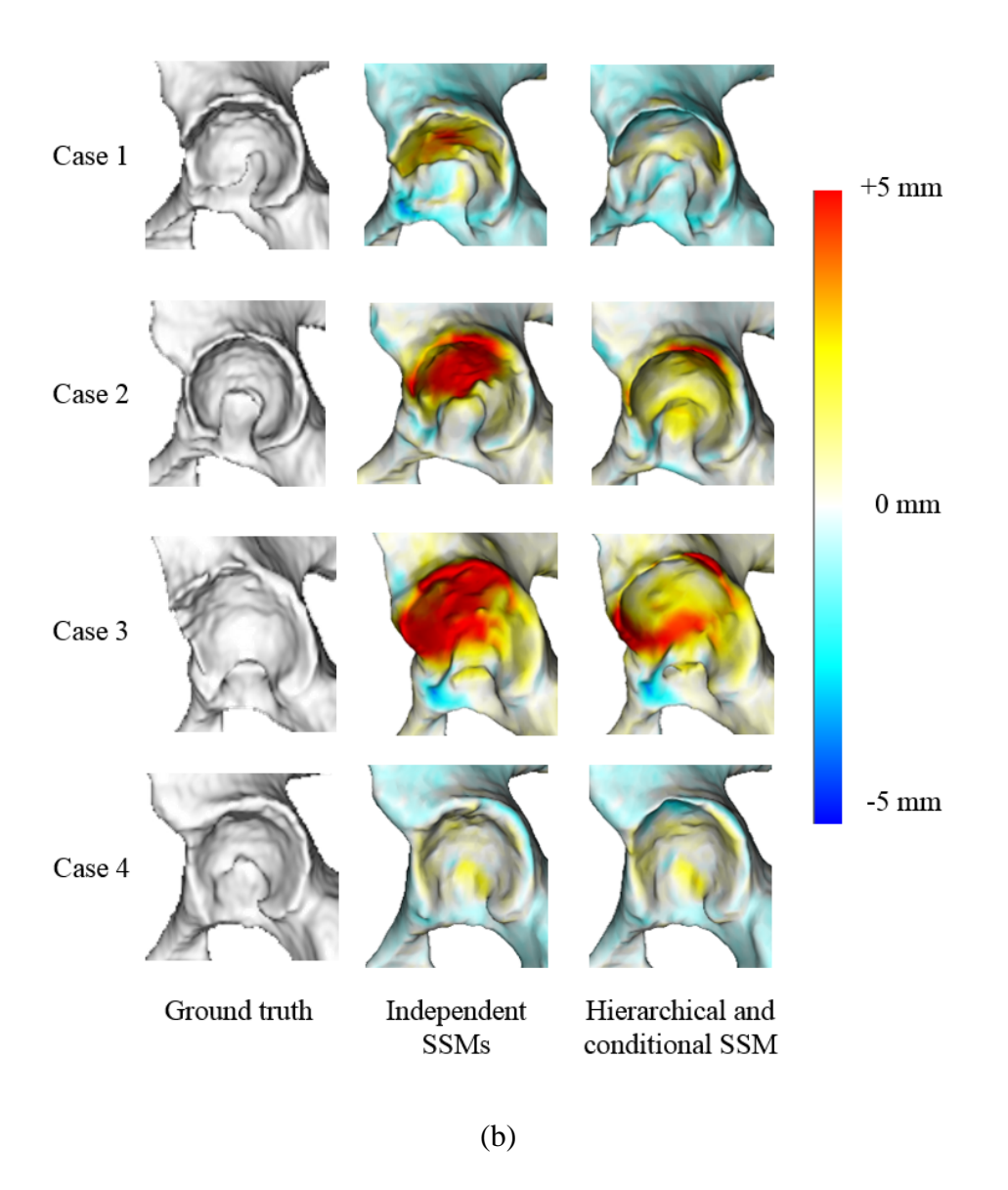


Figure 3.13: Segmentation results of the representative case of each disease category. Case 1, 2, 3, and 4 correspond to osteoarthritis, crowe 1, crowe 2 and collapsed hip, respectively. (a) coronal slices at the plane of the approximate femoral center. The green and red contours correspond to the segmented regions of the pelvis and femur, respectively. Arrows in (a) indicate the part where segmentation accuracy improved with the hierarchical and conditional SSM. (b) and (c) 3D rendering of the segmented surface with colormap indicating the surface distance error.

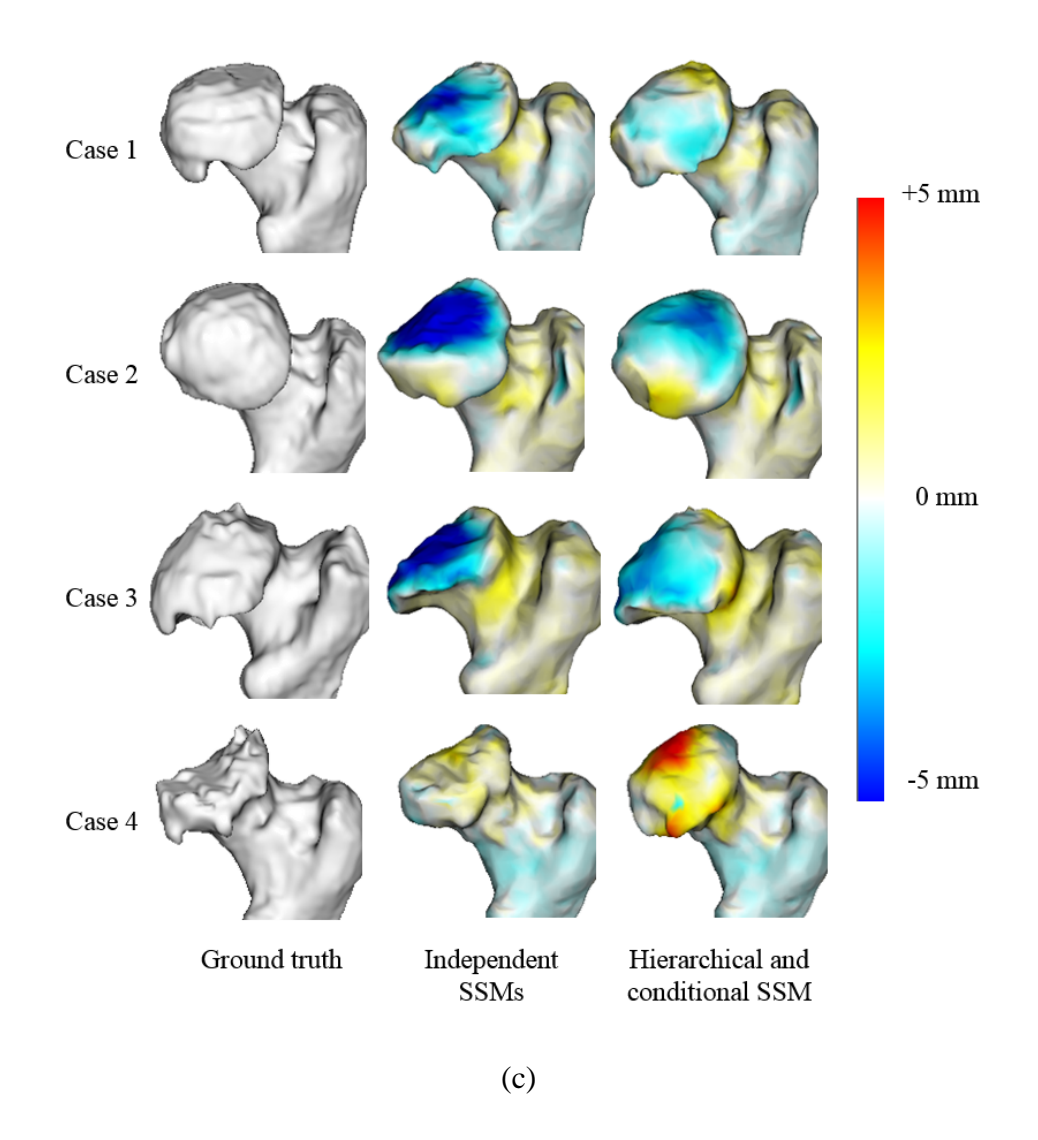


Figure 3.14: Segmentation results of the representative case of each disease category. Case 1, 2, 3, and 4 correspond to osteoarthritis, crowe 1, crowe 2 and collapsed hip, respectively. (a) coronal slices at the plane of the approximate femoral center. The green and red contours correspond to the segmented regions of the pelvis and femur, respectively. Arrows in (a) indicate the part where segmentation accuracy improved with the hierarchical and conditional SSM. (b) and (c) 3D rendering of the segmented surface with colormap indicating the surface distance error.

Table 3.4: Evaluation results for the acetabulum segmentation accuracy of disease category. Mean and standard deviation of ASD [mm] in each category are shown for each method. The best results are shown in bold. * and **: significant improvement; *: 0.01 , **: <math>p < 0.01.

		Primary osteoarthritis	Crowe:1	Crowe: 2, 3, 4	Collapsed hip
Acetabulum	Individual SSMs	1.15±0.36	1.31±0.62	3.39±2.51	1.09±0.29
	Hierarchical SSM	1.06±0.17	1.09±0.54	2.18±1.13	0.88±0.20
	Hierarchical and conditional SSM (Proposed method)	1.08±0.26	1.12±0.59	1.99±1.09	0.87±0.25
Femoral head	Individual SSMs	1.13±0.42	1.41±0.71	2.75±1.15	1.53±0.61
	Hierarchical SSM	0.99±0.37	1.16±0.67	1.87±0.71	1.13±0.38
	Hierarchical and conditional SSM (Proposed method)	0.99±0.22	1.16±0.78	1.84±0.93	1.07±0.42

Computational performance

The total computational times to conduct segmentation for one hemi-hip were 10 min with the individual SSMs, 13 min with the hierarchical SSM, and 15 min with the proposed hierarchical and conditional SSM. The computational times to conduct construction for one hemi-hip were 10 sec for the individual SSM, 20 sec for the hierarchical SSM, and 20 sec for the conditional SSM.

Table 3.5: Evaluation results for segmentation accuracy of whole pelvis and femur. Mean and standard deviation of ASDs over two hundreds dataset are shown in each method. The best results are shown in bold. * and **: significant improvement; *: 0.01 , **: <math>p < 0.01.

	Pelvis		Femur		
	Unaffected	Diseased	Unaffected	Diseased	
Individual SSMs	0.49 ± 0.23	0.58±0.22 ¬*	0.61 ± 0.19	0.71 ± 0.21	
Hierarchical SSM	0.47 ± 0.22	0.54±0.15 [_] ,	0.60±0.22	0.70 ± 0.23	
Hierarchical and		÷	(
conditional SSM	0.47 ± 0.21	0.53±0.15	0.58 ± 0.22	0.70 ± 0.22	
(Proposed method)					

3.6 Discussion

The hierarchical SSM approach significantly improved ASD compared to the approach that simply applied the pelvis SSM and the femur SSM individually, which was referred to as individual SSMs. The SSM containing both pelvis and femur, which was used in the first level of the hierarchical SSM, modeled the surface shape of the pelvis and femur around the joint region based on the joint distribution, resulting in an improved accuracy of the surface estimate. The similar result was obtained in [12], where the joint SSM was used in the first step.

Fig. 6 illustrates the fact that the segmentation of the acetabulum was more accurate than the femoral head (1.32 mm vs 3.46 mm ASD), suggesting that the degree of difficulty of segmentation significantly varies depending on the anatomy even if they are geometrically close to each other. The sequential strategy, where the femoral head was segmented after the acetabulum) improved ASD of the femoral head from 3.46 mm to 1.18 mm. [Yokota: 2009] used the SSM based on the joint distribution and reported the ASD of 1.78 mm, which also indicates that the sequential segmentation strategy based on the segmentation difficulty was

fairly effective in our dataset.

Fig. 4 illustrates the effectiveness of the conditional SSM. The initial shape approximated to patient-specific shape with use of the conditional SSM. Additionally segmentation worked robustly even if the edge information was insufficient by grace of the restriction for the model deformation.

The conditional FH-SSM was most effective in severely worn cases such as Crowe 2 since SSM compensated the obscure edge information, while it was less effective in Crowe 1 and avascular necrosis where the boundary in the image was relatively distinctive. The edge search tended to be trapped in a local optima when generality of the SSM was high in the cases such as the ambiguous edges in Crowe 2. The conditional SSM yielded a positive effect of decreasing generality unnecessary for the particular patient and increasing specificity, which contributed to the improved accuracy.

The segmentation of femoral head has shown to be difficult in general compared to acetabulum in prior works such as [26] even if there is no major abnormal deformity. The error mainly arose from misdetection of the boundary of the femoral head when the algorithm was confused by the cortical bone boundary inside the pelvis and the internal boundary of the pelvis. The individual SSM wrongly fitted at those boundaries due to its high generality, while the proposed conditional SSM with decreased generality successfully detected the correct edges in unaffected hips as well.

The standard deviation of ASD at acetabulum and femoral head within the five trials where the training dataset was randomly selected (see section 4.1 for detail) was fairly small (0.01 mm), indicating that the sensitivity of the segmentation result to the choice of training dataset was small. More comprehensive sensitivity studies against various characteristics of the training dataset (e.g., number of dataset, distribution of disease type) are the subject of future work.

Segmentation failed in some avascular necrosis cases even when the edge was clear be-

cause the model could not represent the severely deformed (e.g., concave) femoral head due to insufficient number of training samples of the particular disease type (10% of the entire sample). This suggests the necessity of the disease-specific SSM. Fig. 12 shows the worst case where the deformation due to the disease was unique, that is the acetabulum would normally deform to dislocate as the disease progresses, reversed deformation was confirmed in this case. Thus the SSM did not have ability to sufficient represent the specific instance beyond the training dataset.

Kainmueller [26] and Schmid [33] reported comparable segmentation errors at the pelvis in healthy subjects, which were 0.6 mm and 1.15 mm respectively. The present work was especially effective for segmentation of the joint surface in diseased hips, which are the most important factor in the preoperative planning and surgical simulation of hip surgeries.

One limitation of the current implementation is that it requires to empirically determine the threshold value. In this study, the thresholds were determined based on the cross-validation tests within the training dataset. The strategy was highly effective since the scanning condition (i.e., intensity calibration, x-ray tube current, voltage, etc.) was fairly uniform across the entire dataset, however, a more flexible strategy to automatically determine the threshold without using the training dataset would be preferable to handle newly acquired datasets of different types of scanner of various hospitals.

Tuning of the two parameters: 1) threshold of p-value to determine the range of conditional SSM and 2) γ as the constraint of the deformation, worked effectively in balancing sensitivity and generality. Since the conditional SSM generally improves sensitivity instead of deteriorating generality, it is not effective to apply it in a broader range over the bone such as using the entire pelvis as the condition for the femur segmentation (this corresponds the case where log10p; -40 in Figure 7). A similar discussion can be held for γ as well, that is an excessive constraint (i.e., larger γ) hinders proper deformation even if the edges are apparent.

Some prior works [56, 57] addressed the segmentation of abdominal organs using an empirically predetermined order (e.g., starts from an organ easier to segment and using the organ as a condition surface). These works defined the condition surface treating each organ as the smallest unit. While we defined it based on statistical analysis which has the advantage mentioned above.

3.7 Conclusions

This thesis proposed a segmentation framework that cascades the hierarchical SSM and conditional SSM to achieve an improved robustness and accuracy specifically in the diseased hip joint. The challenges in hip segmentation of diseased hips that precludes application in clinical routine are the large bone deformity of the bones, and the lack of boundary information around the joint space due to degenerated articular cartilage, which we overcame by the sequential use of the hierarchical SSM and conditional SSM in the proposed framework. The experiments using a well-organized patient database quantitatively demonstrated clinical applicability of the proposed framework in surgical planning, navigation and diagnosis (e.g., understanding of progression of a disease, automatic classification of a disease type).

The contributions of the thesis are the followings. 1) A systematic strategy to sequentially select the segmentation target (i.e., pelvis or femur in the case of hip) based on learning from cross-validation tests within the training dataset, 2) a statistically reasonable (CCA) approach to determine the extent of the conditional surface for construction of the conditional SSM, and 3) extensive validations with CT data of one hundred disease hips categorized by the disease type.

We expect that an SSM using training datasets of only specific disease type [58] which we call "disease-specific SSM" will further improve specificity for target disease type.

A straightforward extension of the proposed method includes application to other types of

joint including the knee, shoulder and vertebra.

Chapter 4

Automated CT Segmentation of MusclesUsing Hierarchical Multi-Atlas method

Abstract

Patient-specific biomechanical simulations using image-based musculoskeletal modeling have been proved to be useful. However, time-consuming nature in image segmentation of muscles is an obstacle to their clinical application. In this thesis, we propose a fully-automated method for segmentation of muscles from hip CT data whose FOV covers the entire pelvis and femur. The feature of the proposed method is hierarchical strategy using hierarchical nature inherent in the musculoskeletal anatomy. The evaluation was performed using the ground truth on three representative 2D axial slices of 10 CT datasets in a leave-one-out manner. The average absolute distance error of segmented 17 muscles was 3.1 mm for the proposed and 4.2 mm for the simplified methods, respectively.

4.1 Introduction

Patient-specific biomechanical simulations using image-based musculoskeletal modeling have been proved to be useful [59]. However, time-consuming nature in image segmentation of muscles is an obstacle to their clinical application. Although previous works tried to automate muscle segmentation, they still involved considerable manual interactions [37] or just approximated muscles as strings instead of segmenting their regions [60]. In this thesis, we propose a fully-automated method for segmentation of muscles from hip CT data whose FOV covers the entire pelvis and femur. The feature of the proposed method is hierarchical strategy using hierarchical nature inherent in the musculoskeletal anatomy. We validate that the hierarchy embedded in the proposed method significantly improves the segmentation accuracy.

4.2 Methods

4.2.1 Overview

Our targets were 17 muscles (including muscle groups) of the hip and thigh. We utilize hierarchical relations among structures in the hip CT images during multi-stage segmentation processes. In our formulation, the hierarchical relations are naturally defined from anatomical hierarchy. These relations also fit to the strategy that easier segmentable regions are extracted at earlier stages while more difficult ones at later stages using the constraints derived from regions extracted at earlier stages.

Based on the above consideration, a multi-stage segmentation approach is formulated. We firstly segment the inside-of-skin (soft tissue) and bones (pelvis, and femur). Secondly the muscle tissue is segmented, given the soft tissue, pelvis, and femur regions. Finally, 17 individual muscles are segmented, given the muscle tissue regions in addition to the regions

used in the previous stage.

The labor of preparing the training dataset is a considerable issue. Especially, we have found that atlas preparation of individual muscles by manual tracing is highly labor-intensive task. Therefore, we aim to develop a method which minimizes the amount of the preparation but still keeps good accuracy. To do so, we select a small number of muscles out of 17 muscles, from which the shape and locations of the remaining muscles are likely to be well-predicted. Additional training datasets are prepared for the selected muscles and utilized to introduce an additional hierarchical level to improve the accuracy. In the following, the details of the methods are described.

4.2.2 Hierarchical multi-atlas label fusion

The multi-atlas label fusion method [61] assumes that multiple atlas datasets consisting of original CT images and their pre-segmented label images of target structures, which we call "target label images" hereafter, are prepared beforehand. Given an input CT image, intensity-based nonrigid registration [50] is performed between the input CT image and that of each atlas dataset to estimate the deformation field, and then the corresponding target label image is deformed using the estimated deformation field to obtain a segmentation result. The different segmentation results for different atlases are fused by their weighted sum whose weights are based on resulted similarity in registration. The fused segmentation result is thresholded to obtain a final segmentation result.

We apply the above method hierarchically. Our hierarchical method assumes that the presegmented label images of reference structures, which we call "reference label images", are prepared in the atlas datasets in addition to the target label images. We also assume that the regions of the reference structures (which we call "reference regions") have already been segmented from an input CT image at the previous stage of automated segmentation processes.

That is, the input dataset consists of the original CT image and (automatically segmented) reference label image. Before the registration of original CT images, nonrigid registration of the reference label images (label-based nonrigid registration) between the input dataset and each atlas is performed to deform each original CT image of the atlas so that the reference structures are registered. This registration is quite stable because the segmented regions are used. It normalizes inter-subject variations of the reference structures, and thus subsequent intensity-based nonrigid registration is stabilized because it only deals with remaining reduced variations mainly originated from the target structures. The segmented target structures are added to the reference label images at the next stage of segmentation processes. This procedure is iterated until the target structures at the final stage are segmented

4.2.3 Application to hip and thigh musculoskeletal segmentation

Figure 4.1 shows a schematic diagram of hip and thigh musculoskeletal segmentation processes using hierarchical multi-atlas label fusion. We firstly segment the regions of the inside-of-skin, pelvis, and femur to use them as the initial reference label image (top left of Fig. 4.1) for the subsequent hierarchical segmentation. The inside-of-skin region is segmented by a simple binarization using a fixed threshold value. The pelvis and femur are segmented using a method similar to [12].

Given the input dataset of an original CT image and the initial reference label image (inside-of-skin, pelvis, and femur), the hierarchical multi-atlas label fusion is applied. At the first stage, the target structure is the muscle tissue (top middle of Fig. 4.1), which is added to the reference structures of the second stage. At the second stage, the targets are four selected muscles (top right of Fig. 4.1), which are added to the references of the final stage, where 17 muscles are segmented out.

In the above procedure, we assume that more than a few atlas datasets are used for the first

and second stages while only a limited number (e.g. one or two) of atlas datasets are used for the final stage. It should be noted that the amount of labor is much smaller in preparing the atlas datasets of muscle tissues for e.g. 20 patients (required at the first stage) than 17 individual muscles for only one patient (required at the final stage) because the interactive graph-cut editing [53] is possible in the former while full manual traces are inevitable in the latter.

4.3 Results

20 patient datasets used for the atlas datasets for muscle tissue segmentation at the first stage while one patient dataset for 17 individual muscle segmentation at the second stage. Because one-side of the hip was diseased in our datasets, there was considerable difference between left and right hemi-hips. 40 and two atlas datasets of the left and mirror-transformed right hemi-hips were used for the first and second stages, respectively. The evaluation was performed using the ground truth on three representative 2D axial slices of 10 CT datasets in a leave-one-out manner. We compared the proposed two-stage method with a simplified single-stage method without muscle tissue segmentation. These methods were fully-automated. Fig. 4.2(c) and (d) show typical results of individual muscle segmentation. The average absolute distance error of segmented 17 muscles was 3.1 mm for the proposed and 4.2 mm for the simplified methods, respectively. In 8 out of 17 muscles, the proposed method was significantly accurate (p_i0.01) (no significance in 9muscles). These results show that the hierarchy embedded in the proposed method was quite effective.

4.4 Discussion and conclusions

We have described a method for muscle segmentation from CT data. By adding intermediate muscle tissue segmentation in the proposed hierarchical method, segmentation accuracy was significantly improved. This addition was also effective with respect to the amount of labor, which was much less in preparing the atlas datasets of muscle tissues for 20 cases than 17 individual muscles for only one case because the interactive graph-cut editing is possible in the former while full manual traces are inevitable in the latter. As future work, we will add another intermediate stage of segmenting a few individual muscles using 20 patient atlas datasets so as to improve the accuracy.

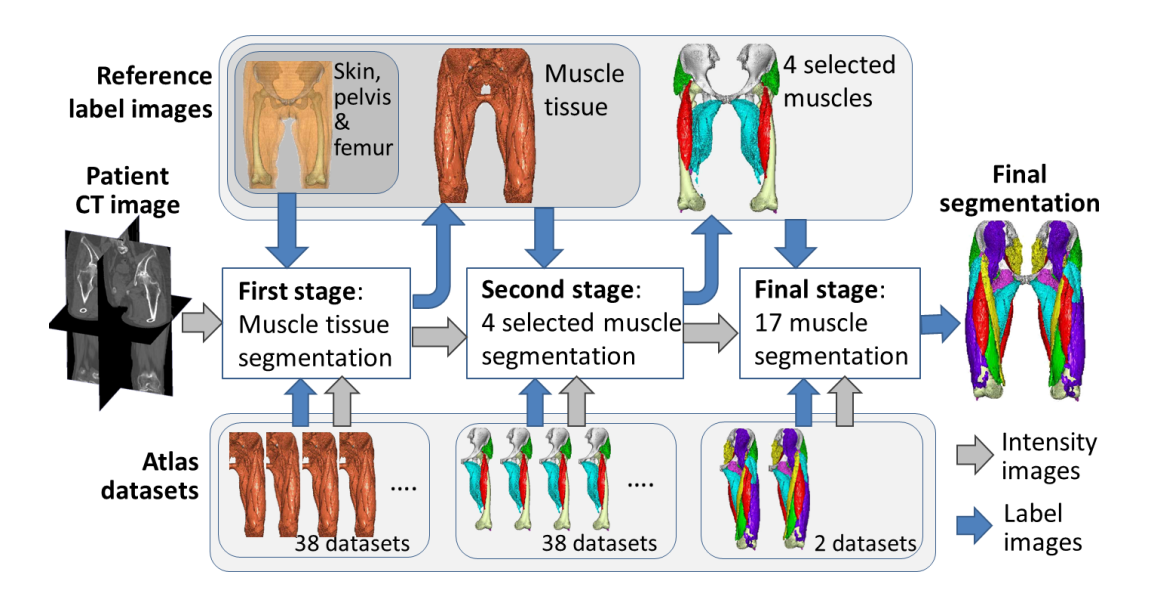


Figure 4.1: Schematic diagram of hip and thigh musculoskeletal segmentation processes using hierarchical multi-atlas label fusion.

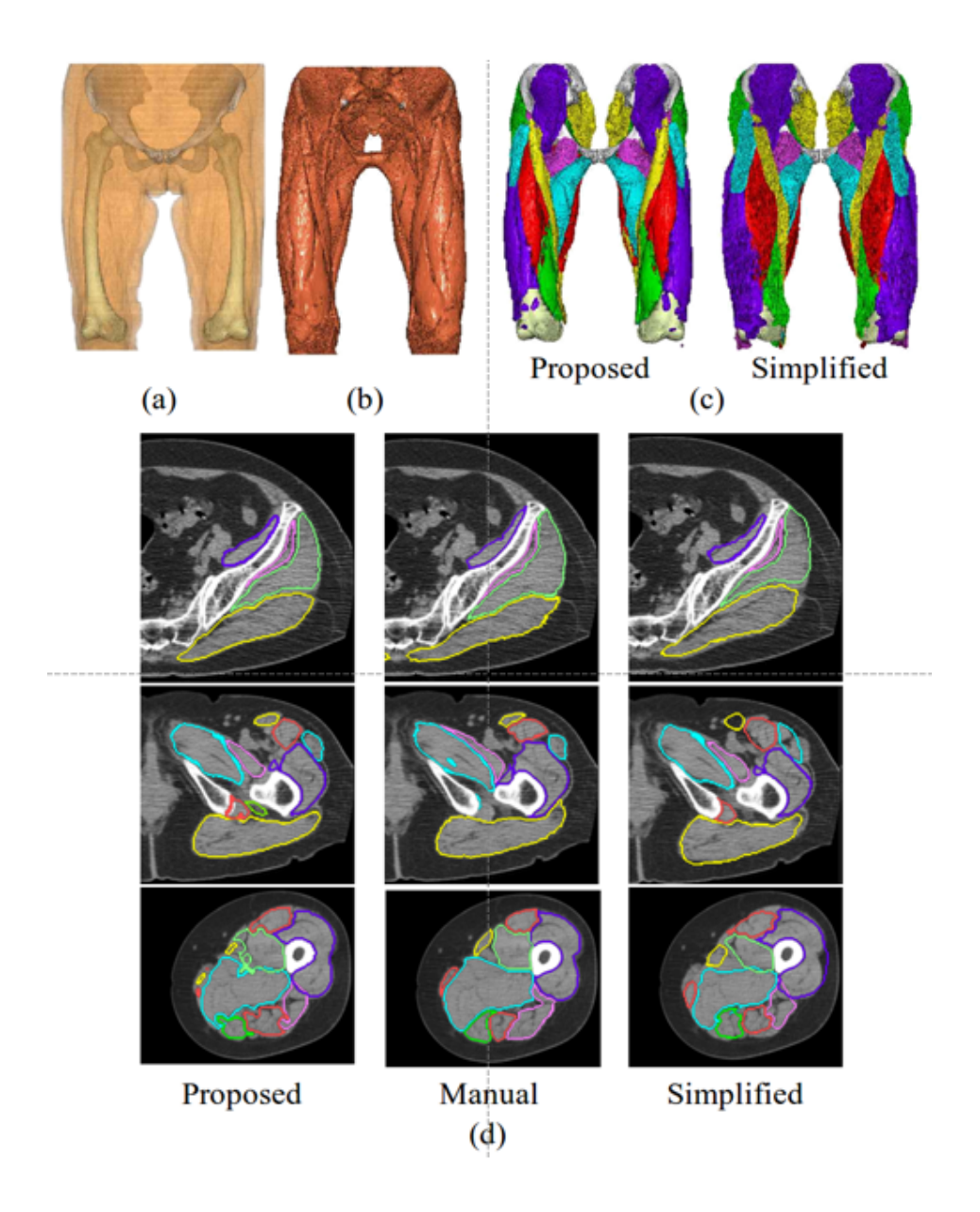


Figure 4.2: Typical cases of muscle segmentation. (a) Body (skin), pelvis, and femur. (b) Muscle tissues. (c) 17 individual muscles. Left: Proposed method. Right: Simplified method. (d) Axial slices of segmentation results of individual muscles. Left: Proposed method. Middle: Manual traces. Right: Simplified method.

Chapter 5

Conclusions

In this thesis, I accomplished an automated segmentation of the bones and muscles in the hip and thigh from x-ray computed tomography. Recognition of the anatomical landmarks is described in chapter 2. Segmentation of the bones (pelvis and femur) is described in chapter 3. Segmentation of the muscles (seventeen individual muscles) is described in Chapter 4.

The proposed method was based on a statistical atlas derived from a group of individuals, therefore, the training dataset needs to be carefully selected in a way such that the population contains the target patient. In this thesis, the training dataset consists of the Japanese female patients who underwent THA. As is the case for any study on the statistical learning based method, an extensive validation with a significant amount of population dataset will be needed to prove the generalizability of the experimental result. The validation with different population demography (e.g. male, different disease type or race) is in the scope of our future work.

Our future work also includes: 1) application to different anatomies (e.g. knee, shoulder, etc.) and different modalities (e.g. MRI), 2) application to the musculoskeletal simulation including a model of muscle fibers and considering the porosity difference between cortical bone and trabecular bone that may be obtained from a series of photos of a thin sectioned frozen specimen such as the one created in Visible Korean Human project [62] (Fig. 5.1).

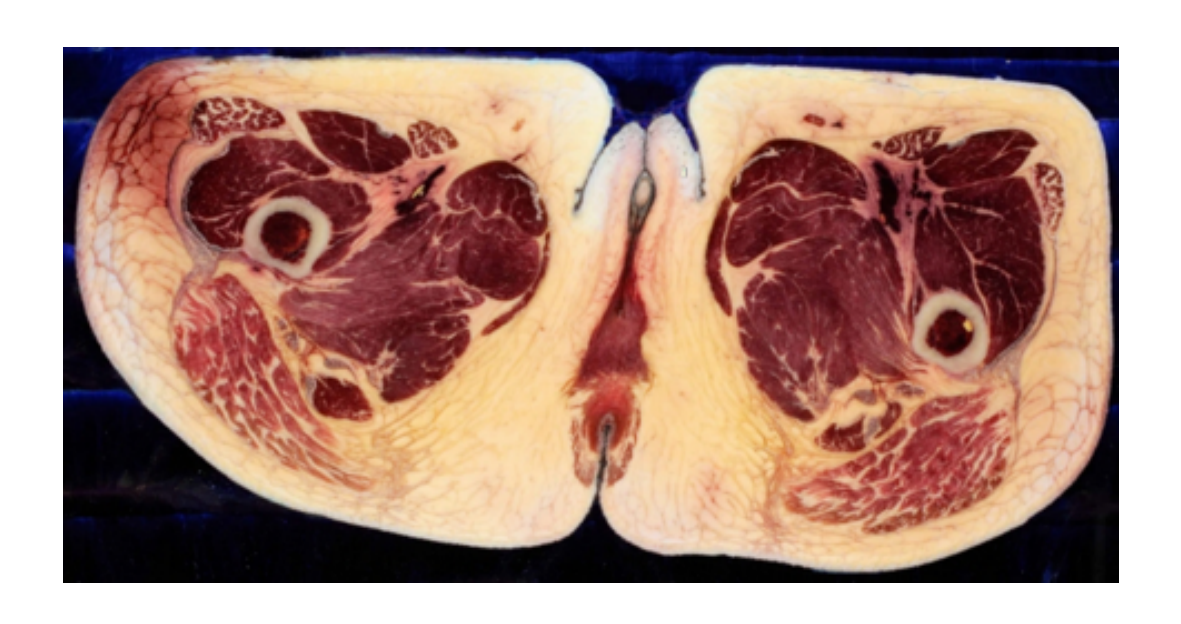


Figure 5.1: An example sectioned slice in Visible Korean Human (VKH).

Acknowledgements

The author would like to give special thanks to Professor Yukio Tada of Graduate School of System Informatics, Kobe University, for his kind advices, discussions and guidance.

The author would like to give special thanks to Professor Yasuo Ariki, and Professor Toshiya Kaihara for their efforts for reviewing this doctoral dissertation.

The author also would like to appreciate to Professor Yoshinobu Sato, Associate Professor Yoshito Otake of Graduate School of Information Science, Nara Institute of Technology and Science and Dr. Masahiko Nakamoto of the EBM Corporation and Assistant Professor Toshiyuki Okada of the Department of Surgery, Faculty of Medicine, University of Tsukuba for their precious advices and instructions about this study.

The author would like to thank to Associate Professor Kazuyuki Hanahara, Assistant Professor Takateru Urakubo of Graduate School of System Informatics, Kobe University for their guidance and instructions.

The author would like to thank to Professor Nobuhiko Sugano of the Department of Orthopaedic Medical Engineering, Graduate School of Medicine, Osaka University and Assistant Professor Masaki Takao and Dr. Takeshi Ogawa of the Department of Organ Regulation Medicine, Graduate School of Medicine, Osaka University for their support, discussion from clinical aspects and providing CT images of the hip.

The author would like to thank to Assistant Professor Yoshiyuki Kagiyama of the Interdisciplinary Graduate School of Medicine and Engineering, Yamanashi University for his precious advices, discussions and encouragements about this study.

The author would like to thank to Ms. Yuki Nakanishi of Graduate School of System Informatics, Kobe University for her cooperative activity and encouragements about this study.

The author thanks to all the members of CS-22 Tada Laboratory of the Graduate School of System Informatics, Kobe University and the Imaging-based Computational Biomedicine Laboratory, Graduate School of Information Science, Nara Institute of Technology and Sci-

ence.

Finally, I would like to thank to my family, and all of my friends for ungrudging support for my academic life.

Bibliography

- [1] VPHOP. "The Osteoporotic Virtual Physiological Human", (2010)
- [2] J. D. Webb, S. S. Blemker, and S. L. Delp, "3D finite element models of shoulder muscles for computing lines of actions and moment arms.", *Computer methods in biomechanics and biomedical engineering*, 17(8), 829–37January, (2014)
- [3] Voxel-Man. "Voxel-Man", (2014)
- [4] M. Blauth, R. Schubert, and A. Frangi, "A statistical model of shape and bone mineral density distribution of the proximal femur for fracture risk assessment", *Image Computing and*, 14(Pt 2), 393–400January, (2011)
- [5] I. Otomaru, M. Nakamoto, Y. Kagiyama, M. Takao, N. Sugano, N. Tomiyama, Y. Tada, and Y. Sato, "Automated preoperative planning of femoral stem in total hip arthroplasty from 3D CT data: atlas-based approach and comparative study.", *Medical image analysis*, 16(2), 415–26February, (2012)
- [6] Y. Kagiyama, M. Takao, M. Nakamoto, N. Sugano, H. Yoshikawa, O. Oshiro, Y. Tada, and Y. Sato, "Automated Integration Procedure for Pelvic and Femoral Planning Based on Joint Function Evaluation in Total Hip Replacement", *Transactions of Japanese Society for Medical and Biological Engineering*, 47(1), 88–98, (2002)

- [7] F. Gelaude, T. Clijmans, and H. Delport, "Quantitative Computerized Assessment of the Degree of Acetabular Bone Deficiency: Total radial Acetabular Bone Loss (TrABL).", Advances in orthopedics, 2011, 494382January, (2011)
- [8] J. Kohout, G. Clapworthy, S. Martelli, and M. Vieconti. "Muscle fibres modelling". In *GRAPP/IVAPP*, 58–66, (2012)
- [9] K. H. Höhne, B. Pflesser, A. Pommert, K. Priesmeyer, M. Riemer, T. Schiemann, R. Schubert, U. Tiede, H. Frederking, S. Gehrmann, et al. VOXEL-MAN 3D-Navigator: inner organs: regional, systemic and radiological anatomy. Springer, (2000)
- [10] D. Murray, "The definition and measurement of acetabular orientation", *Journal of Bone & Joint Surgery, British Volume*, 75(2), 228–232, (1993)
- [11] H. Miki, W. Yamanashi, T. Nishii, Y. Sato, H. Yoshikawa, and N. Sugano, "Anatomic hip range of motion after implantation during total hip arthroplasty as measured by a navigation system.", *The Journal of arthroplasty*, 22(7), 946–52October, (2007)
- [12] F. Yokota, T. Okada, M. Takao, N. Sugano, Y. Tada, Y. Sato, and Yokota, "Automated Segmentation of the Femur and Pelvis from 3D CT Data of Diseased Hip Using Hierarchical Statistical Shape Model of Joint Structure", *Lecture Notes in Computer Science*, 5762, 811–818January, (2009)
- [13] S. Kobashi, S. Fujimoto, T. Nishiyama, N. Kanzaki, T. Fujishiro, N. Shibanuma, K. Kuramoto, M. Kurosaka, and Y. Hata, "Robust pelvic coordinate system determination for pose changes in multidetector-row computed tomography image", *INTERNATIONAL JOURNAL of FUZZY LOGIC and INTELLIGENT SYSTEMS*, 10(1), 65—72, (2010)
- [14] J. Ehrhardt, H. Handels, B. Strathmann, T. Malina, W. Plötz, and S. J. Pöppl, "Atlasbased recognition of anatomical structures and landmarks and the automatic computa-

- tion of orthopedic parameters", *Methods of Information in Medicine*, 43(4), 391–397, (2004)
- [15] T. Cootes, C. Taylor, D. Cooper, and J. Graham, "Active shape models-their training and application", *Computer vision and image*..., 61, (1995)
- [16] P. Foroughi, D. Song, and G. Chintalapani, "Localization of pelvic anatomical coordinate system using US/atlas registration for total hip replacement", ... *Image Computing* and ..., 5242, 871–879, (2008)
- [17] X. Zhou, T. Kitagawa, T. Hara, H. Fujita, X. Zhang, R. Yokoyama, H. Kondo, M. Kanematsu, and H. Hoshi, "Constructing a probabilistic model for automated liver region segmentation using non-contrast X-ray torso CT images.", *Lecture Notes in Computer Science*, 4191, 856–63January, (2006)
- [18] B. M. DiGioia AM, Jaramaz B, "The ottoaufranc award. image guided navigation system to measure intraoperatively acetabular implant alignment", *Clin Orthop Relat Res.*, 355, 8—-22, (1998)
- [19] V. Wiwanitkit, "ISB recommendation on definitions of joint coordinate system of various joints for the reporting of human joint motion part I: ankle, hip, and spine", JONA'S healthcare law, ethics and regulation, 12(4), 88, (2002)
- [20] S. Nishihara, N. Sugano, T. Nishii, K. Ohzono, and H. Yoshikawa, "Measurements of pelvic flexion angle using three-dimensional computed tomography.", *Clinical orthopaedics and related research*, 140–151, (2003)
- [21] F. Gelaude, T. Clijmans, and H. Delport, "Quantitative Computerized Assessment of the Degree of Acetabular Bone Deficiency: Total radial Acetabular Bone Loss (TrABL).", Advances in orthopedics, 2011, 494382January, (2011)

- [22] Y. Kagiyama, M. Takao, M. Nakamoto, Y. Sato, N. Sugano, H. Yoshikawa, K. Akazawa, S. Tamura, and Y. Tada, "Automated planning of multi-component implants for THA using multiple criteria including limb length and range of motion", *International Journal of Computer Assisted Radiology and Surgery*, 1(S1), 232–234June, (2006)
- [23] C. Potratz, D. Kluess, H. Ewald, and U. v. Rienen, "Multiobjective optimization of an electrostimulative acetabular revision system.", *IEEE transactions on bio-medical engineering*, 57(2), 460–8February, (2010)
- [24] S. S. Chandra, Y. Xia, C. Engstrom, S. Crozier, R. Schwarz, and J. Fripp, "Focused Shape Models for Hip Joint Segmentation in 3D Magnetic Resonance Images", *Medical Image Analysis*February, (2014)
- [25] B. Haas, T. Coradi, M. Scholz, P. Kunz, M. Huber, U. Oppitz, L. André, V. Lengkeek, D. Huyskens, A. v. Esch, and R. Reddick, "Automatic segmentation of thoracic and pelvic CT images for radiotherapy planning using implicit anatomic knowledge and organ-specific segmentation strategies.", *Physics in medicine and biology*, 53(6), 1751–71March, (2008)
- [26] D. Kainmueller, H. Lamecker, S. Zachow, and H.-C. Hege. "An articulated statistical shape model for accurate hip joint segmentation.". In *Conference proceedings : ...*Annual International Conference of the IEEE Engineering in Medicine and Biology Society. IEEE Engineering in Medicine and Biology Society. Conference, 6345–51January, (2009)
- [27] Y. Kang and K. Engelke, "A new accurate and precise 3-D segmentation method for skeletal structures in volumetric CT data", *Medical Imaging, IEEE*, 22(5), 586–98May , (2003)

- [28] J. Pettersson and H. Knutsson, "Automatic hip bone segmentation using non-rigid registration", *Pattern Recognition*, 2006., 946–949, (2006)
- [29] J. Schmid, J. Kim, and N. Magnenat-Thalmann, "Extreme leg motion analysis of professional ballet dancers via MRI segmentation of multiple leg postures.", *International journal of computer assisted radiology and surgery*, 6(1), 47–57January, (2011)
- [30] R. a. Zoroofi, Y. Sato, T. Sasama, T. Nishii, N. Sugano, K. Yonenobu, H. Yoshikawa, T. Ochi, and S. Tamura, "Automated segmentation of acetabulum and femoral head from 3-D CT images.", *IEEE transactions on information technology in biomedicine* : a publication of the IEEE Engineering in Medicine and Biology Society, 7(4), 329–43December, (2003)
- [31] G. T. ONeill, W.-S. Lee, and P. Beaulé, "Segmentation of cam-type femurs from CT scans", *The Visual Computer*, 28(2), 205–218October, (2011)
- [32] A. Akhondi-Asl, L. Hoyte, M. Lockhart, and S. Warfield, "A Logarithmic Opinion Pool Based STAPLE Algorithm for the Fusion of Segmentations With Associated Reliability Weights.", *IEEE transactions on medical imaging*, 0062(c), 1–14June, (2014)
- [33] J. Schmid and J. Kim, "Coupled registration-segmentation: application to femur analysis with intra-subject multiple levels of detail MRI data", *Medical Image Computing* and, 13(Pt 2), 562–9January, (2010)
- [34] L. Liu, D. Raber, D. Nopachai, P. Commean, D. Sinacore, F. Prior, R. Pless, and T. Ju, "Interactive separation of segmented bones in CT volumes using graph cut.", *Medical image computing and computer-assisted intervention : MICCAI ... International Conference on Medical Image Computing and Computer-Assisted Intervention*, 11(Pt 1), 296–304January, (2008)

- [35] L. Ben Younes, Y. Nakajima, and T. Saito, "Fully automatic segmentation of the Femur from 3D-CT images using primitive shape recognition and statistical shape models.", *International journal of computer assisted radiology and surgery*October, (2013)
- [36] H. Seim, D. Kainmueller, M. Heller, H. Lamecker, S. Zachow, and H. Hege. "Automatic segmentation of the pelvic bones from ct data based on a statistical shape model".
 In Eurographics Workshop on Visual Computing for Biomedicine, 93–100, (2008)
- [37] B. Gilles and N. Magnenat-Thalmann, "Musculoskeletal MRI segmentation using multi-resolution simplex meshes with medial representations.", *Medical image analysis*, 14(3), 291–302June, (2010)
- [38] D. Kainmueller, H. Lamecker, S. Zachow, and H. Hege. "Coupling Deformable Models for Multi-object Segmentation". In *Proceedings of the 4th international symposium on Biomedical Simulation*, 34–38, (2008)
- [39] M. D. Bruijne, M. T. M. Lund, L. B. L. Tankó, M. d. Bruijne, P. C. Pettersen, and M. Nielsen, "Quantitative vertebral morphometry using neighbor-conditional shape models.", *Medical image analysis*, 11(5), 503–12October, (2007)
- [40] T. Albrecht, R. Knothe, and T. Vetter. "Modeling the Remaining Flexibility of Partially Fixed Statistical Shape Models". In 2nd MICCAI Workshop on Mathematical Foundations of Computational Anatomy, 160–169, (2008)
- [41] E. Syrkina, R. Blanc, and G. Székely, "Propagating uncertainties in statistical model based shape prediction", *SPIE Medical*..., (2011)
- [42] R. Blanc, C. Seiler, G. Székely, L.-P. Nolte, and M. Reyes, "Statistical model based shape prediction from a combination of direct observations and various surrogates:

- application to orthopaedic research.", *Medical image analysis*, 16(6), 1156–66August , (2012)
- [43] Y. M. Yang, D. Rueckert, and A. M. J. Bull, "Predicting the shapes of bones at a joint: application to the shoulder", *Computer Methods in Biomechanics and Biomedical Engineering*, 11(1), 19–30February, (2008)
- [44] C. Davatzikos, X. Tao, and D. Shen, "Hierarchical active shape models, using the wavelet transform.", *IEEE transactions on medical imaging*, 22(3), 414–23March, (2003)
- [45] P. Fillard, X. Pennec, P. M. Thompson, and N. Ayache. "Evaluating brain anatomical correlations via canonical correlation analysis of sulcal Xavier Pennec and Pierre Fillard lines". In *In Proc. of MICCAI'07 Workshop on Statistical Registration: Pair-wise and Group-wise Alignment and Atlas Formation*, (2007)
- [46] F. Yokota, T. Okada, M. Takao, and N. Sugano. "Automated CT Segmentation of Diseased Hip Using Hierarchical and Conditional Statistical Shape Models". In *Medical image computing and computer-assisted intervention : MICCAI ... International Conference on Medical Image Computing and Computer-Assisted Intervention*, 190–197, (2013)
- [47] F. Yokota, T. Okada, M. Takao, N. Sugano, Y. Tada, N. Tomiyama, and Y. Sato, "Automated Localization of Pelvic Anatomical Coordinate System from 3D CT Data of the Hip Using Statistical Atlas", *Medical Imaging Technology*, 30(1), 43–52, (2012)
- [48] T. Okada, R. Shimada, M. Hori, M. Nakamoto, Y.-W. Chen, H. Nakamura, and Y. Sato, "Automated segmentation of the liver from 3D CT images using probabilistic atlas and multilevel statistical shape model.", *Academic radiology*, 15(11), 1390–403November, (2008)

- [49] T. Heimann and H.-P. Meinzer, "Statistical shape models for 3D medical image segmentation: a review.", *Medical image analysis*, 13(4), 543–63August, (2009)
- [50] D. Rueckert, L. I. Sonoda, C. Hayes, D. L. Hill, M. O. Leach, and D. J. Hawkes, "Non-rigid registration using free-form deformations: application to breast MR images.", IEEE transactions on medical imaging, 18(8), 712–21August, (1999)
- [51] H. Lamecker, T. Lange, and M. Seebass, "Segmentation of the liver using a 3D statistical shape model", *Technical report, Zuse Institue*, 09(April), (2004)
- [52] T. Okada. Organ shape recovery from three-dimensional medical images based on anatomical knowledge. PhD thesis, Osaka University, (2010)
- [53] Y. Boykov and M.-P. Jolly, "Interactive graph cuts for optimal boundary & region segmentation of objects in N-D images", *Proceedings Eighth IEEE International Conference on Computer Vision. ICCV 2001*, 1, 105–112, (2001)
- [54] M. S. T. Heimann, B. Ginneken. "MICCAI workshop on 3D segmentation in the clinic."
- [55] D. Rueckert. "Image Registration Toolkit", (2009)
- [56] M. Hammon, A. Cavallaro, M. Erdt, P. Dankerl, M. Kirschner, K. Drechsler, S. Wesarg, M. Uder, and R. Janka, "Model-based pancreas segmentation in portal venous phase contrast-enhanced CT images.", *Journal of digital imaging*, 26(6), 1082–90December , (2013)
- [57] T. Okada, M. G. Linguraru, M. Hori, R. M. Summers, N. Tomiyama, and Y. Sato, "Abdominal multi-organ CT segmentation using organ correlation graph and prediction-based shape and location priors.", *Medical image computing and computer-assisted*

- intervention: MICCAI ... International Conference on Medical Image Computing and Computer-Assisted Intervention, 16(Pt 3), 275–82January, (2013)
- [58] D. P. Mukherjee, K. Higashiura, T. Okada, M. Hori, Y.-W. Chen, N. Tomiyama, and Y. Sato, "Utilizing disease-specific organ shape components for disease discrimination: application to discrimination of chronic liver disease from CT data.", *Lecture Notes in Computer Science*, 8149(Pt 1), 235–42January, (2013)
- [59] C. E. Draper, J. M. Santos, L. C. Kourtis, T. F. Besier, M. Fredericson, G. S. Beaupre, G. E. Gold, and S. L. Delp, "Feasibility of using real-time MRI to measure joint kinematics in 1.5T and open-bore 0.5T systems.", *Journal of magnetic resonance imaging* : *JMRI*, 28(1), 158–66July, (2008)
- [60] L. Scheys, A. Spaepen, P. Suetens, and I. Jonkers, "Calculated moment-arm and muscle-tendon lengths during gait differ substantially using MR based versus rescaled generic lower-limb musculoskeletal models.", *Gait & posture*, 28(4), 640–8November , (2008)
- [61] I. Isgum, M. Staring, A. Rutten, M. Prokop, M. a. Viergever, and B. v. Ginneken, "Multi-atlas-based segmentation with local decision fusion—application to cardiac and aortic segmentation in CT scans.", *IEEE transactions on medical imaging*, 28(7), 1000—10July, (2009)
- [62] J. S. Park, M. S. Chung, S. B. Hwang, B.-S. Shin, and H. S. Park, "Visible Korean Human: its techniques and applications.", *Clinical anatomy (New York, N.Y.)*, 19(3), 216–24April, (2006)

Doctor Thesis, Kobe University

"Automated Segmentation of Bones and Muscles in the Hip and Thigh from X-ray Computed Tomography Scans", 90 pages

Submitted on January, 23, 2015

The date of publication is printed in cover of repositoryversion published in Kobe University Repository Kernel.

© Futoshi Yokota All Right Reserved, 2015